Quantification of the Bed-scale Architecture of Submarine Depositional Environments and Application to Lobe Deposits of the Point Loma Formation, California

Rosemarie C. Fryer and Zane R. Jobe

Department of Geology and Geological Engineering, Colorado School of Mines, Golden Colorado 80401

Abstract

Submarine-fan deposits form the largest sediment accumulations on Earth and host significant reservoirs for hydrocarbons. While many studies of ancient fan deposits qualitatively describe lateral architectural variability (e.g., axis-to-fringe, proximal-to-distal), these relationships are rarely quantified. In order to enable comparison of key relationships that control the lateral architecture of submarine depositional environments, we digitized published bed-scale outcrop correlation panels from five different environments (channel, levee, lobe, channel-lobe-transition-zone, basin plain). Measured architectural parameters (bed thickness, bed thinning rates, lateral correlation distance, net-to-gross) provide a quantitative framework to compare lithology architectures between environments. The results show that sandstone and/or mudstone bed thickness alone or net-to-gross do not reliably differentiate between environments. Lobe sub-environments display the most variability in all parameters, which could be partially caused by subjectivity of qualitative interpretations of environment and demonstrates the need for more quantitative studies of bed-scale heterogeneity. These results can be used to constrain forward stratigraphic models and reservoir models of submarine depositional environments.

This work is paired with a case study to refine the depositional environment of submarine lobe strata of the Upper Cretaceous Point Loma Formation at Cabrillo National Monument near San Diego, California. The strike-oriented, laterally-extensive exposure offers a rare opportunity to observe bed-scale architecture in turbidites over 1 km lateral distance. Thinning rates and bed thicknesses are not statistically different between lobe elements. This signifies that the lateral exposure is necessary to distinguish lobe elements and it would be extremely difficult to accurately interpret elements in the subsurface using 1D data (e.g., core). The grain size, mudstone to sandstone bed thicknesses, and element/bed compensation observed in the Cabrillo National Monument exposures of the Point Loma Formation are most similar to values of semiconfined lobe deposits; hence, we reinterpret that these exposures occupy a more medial position, perhaps with some degree of confinement.

Introduction

Submarine-fan deposits form significant hydrocarbon reservoirs due to their large areal extents and high sand content; however, their internal architecture is poorly quantified (Pettingill & Weimer, 2002; Weimer & Pettingill, 2007). Submarine fans are composed of multiple environments, such as channels, levees, channel lobe transition zones, lobes, and basin plains. Each environment is commonly associated with a particular geometry, facies, and bed thickness distribution (Mutti and Normark, 1987; Normark, 1978; Sullivan et al., 2000; Deptuck et al., 2008; Prélat et al., 2009; Hubbard et al., 2014; Stevenson et al., 2015). For example, submarine lobe deposits typically show a qualitative decrease in bed thickness, grain size, sand content, and amalgamation in proximal-to-distal and axis-to-margin transects (Normark, 1978; Sullivan et al., 2000; Deptuck et al., 2008; Prélat et al., 2009). However, the details of these downstream and lateral facies changes are often overlooked, and very few studies perform correlations at the bed scale (e.g., Chapin and Tiller, 2007; Marini et al., 2015). Even fewer studies have compiled quantitative statistics on bed-scale facies variability (Clark, 1998; Bersezio et al., 2009; Marini et al., 2015; Tőkés and Pattacci, in press). Because event-beds (i.e., turbidites) are the building blocks of submarine depositional environments, these statistics need to be quantified to understand the linkages between geomorphology and stratigraphy, and how turbidity currents are responding to a seafloor that is continually modified by previous deposits (Prélat et al., 2009; Romans et al., 2009; Jobe et al., 2017). Furthermore, in order to understand complex reservoir architectures and vertical/lateral connectivity in submarine fan-deposit reservoirs, these statistics need to be quantified for both the reservoir facies (i.e., sandstone beds) and the potential baffles and barriers (i.e., mudstone/shale beds) (Weber, 1982; Hazeu et al., 1988; Schuppers, 1993; Stephen et al., 2001; Pyrcz et al., 2005). This fine-scale heterogeneity is particularly important in tight-oil developments hosted in submarine lobe deposits (e.g., Permian, Wilcox, the North Sea, West Africa) (Kerans et al., 1994; Haughton et al., 2009; Kane and Ponten, 2012).

In this study, we pair a newly compiled database (from published bed-scale correlation panels) to compare event bed parameters (e.g. bed thickness, bed and facies thinning rates, net-to-gross) of different submarine depositional environments (channels, channel-lobe-transition zones, lobes, levees, and basin plains) with a detailed bed-scale study of submarine lobe deposits of the Point Loma Formation (San Diego, California). These comparisons enable the recognition of (1) architectural similarities and differences between environments and (2) sub-environments within lobe environments (e.g., medial vs. distal, confined vs. unconfined). This analysis provides quantitative and statistical insights into lateral variability within and among submarine depositional environments and provides quantitative data for constructing realistic geologic and reservoir models, particularly in data-poor settings where lateral facies variability at the bed-scale is not observable and a major uncertainty (Hofstra et al., 2017).

Methodology

Compilation Database

In order to enable comparison of multiple depositional environments, we collected bed geometries from publications containing bed-scale correlations from various submarine depositional environments (Figure 1; Table 1). This database consists of 2251 event beds (N) from 56 correlation panels that represent 17 different formations from outcrops around the world (Figure 1; Table 1). We broadly categorized each panel into a depositional environment (channel, levee, channel-lobe transition zone (CLTZ), lobe or basin plain; Table 1). We chose this scheme for simplicity of comparison, and generally my interpretation is in agreement with the original author's interpretation (Table 1). We also associated each panel with a broad paleocurrent panel orientation (strike vs. dip) but did not attempt a correction, because testing indicates that corrections introduce more uncertainty. For example, applying a correction would correctly change the lateral correlation distance, but would incorrectly adjust bed thickness because there is no available information to constrain how bed thickness changes to the new position (i.e., no outcrop constraint; see Supplemental Material A for rationale).

For lobe deposits, we also associated each panel with an interpretation of lobe position (e.g., proximal, medial, distal) and a confinement rating (0 – unconfined, 1 – semi-confined, 2 – confined) based on contextual information and the original author's interpretation. For lobe deposits, we use 'effective confinement' (Brunt et al., 2004) and define categories as the following: an 'unconfined lobe' as the incoming flow has no lateral or distal barriers and is able to freely expand (e.g., Jegou et al., 2008; Picot et al., 2016); a 'semiconfined lobe' has some degree of a lateral or frontal barrier, but the flow is able to freely expand distally or laterally, respectively (e.g., Prather et al., 1998; Marini et al., 2015; the "frontally or laterally confined lobes” of Tőkés and Pattacci, in press); a ‘confined lobe’ has barriers in all directions, which are able to fully contain the flow (e.g., Lamb et al., 2006; Sylvester et al., 2015; the “ponded lobe” of Tőkés and Pattacci, in press).

For each panel, we digitized each event bed with assigned lithology (e.g., turbidite sandstone, turbidite mudstone, debrite) and computed bed thicknesses, thinning rates, net-to-gross, and pinch-outs. Bed thicknesses and net-to-gross values were collected only at measure section locations. We excluded debrite lithologies from the bed-scale analysis due to low sample numbers. We did not collect grain size data because some panels have no grain size information and many panels measure and draw grain size differently, making a comprehensive comparison difficult.

As with any data compilation, some assumptions and interpretations are necessary (e.g., Tőkés and Pattacci, in press). The major assumptions here consist of bed thickness constraints, interpretation of lateral continuity, and assignment of environment. The calculated bed thickness data are skewed towards thicker (>10 cm) beds due to ease of correlation as compared to thinner beds, causing an underestimate in net-to-gross values and higher characteristic bed thickness per environment. This also causes lumping of multiple lithologies (e.g. thin-bedded sands within a dominantly muddy package). However, this occurs across all depositional environments, so we did not apply any correction to individual environments. We also did not correct for outcrop orientation relative to paleoflow because outcrops generally do not provide enough information to decrease uncertainty (Supplemental Material A). Bed thickness and geometry in channelized deposits are commonly poorly constrained due to amalgamation that makes lateral correlation difficult (e.g., Hubbard et al., 2014). In my dataset, this likely causes an overestimate in bed thickness and thus a lower associated thinning rate. To minimize this error for channelized

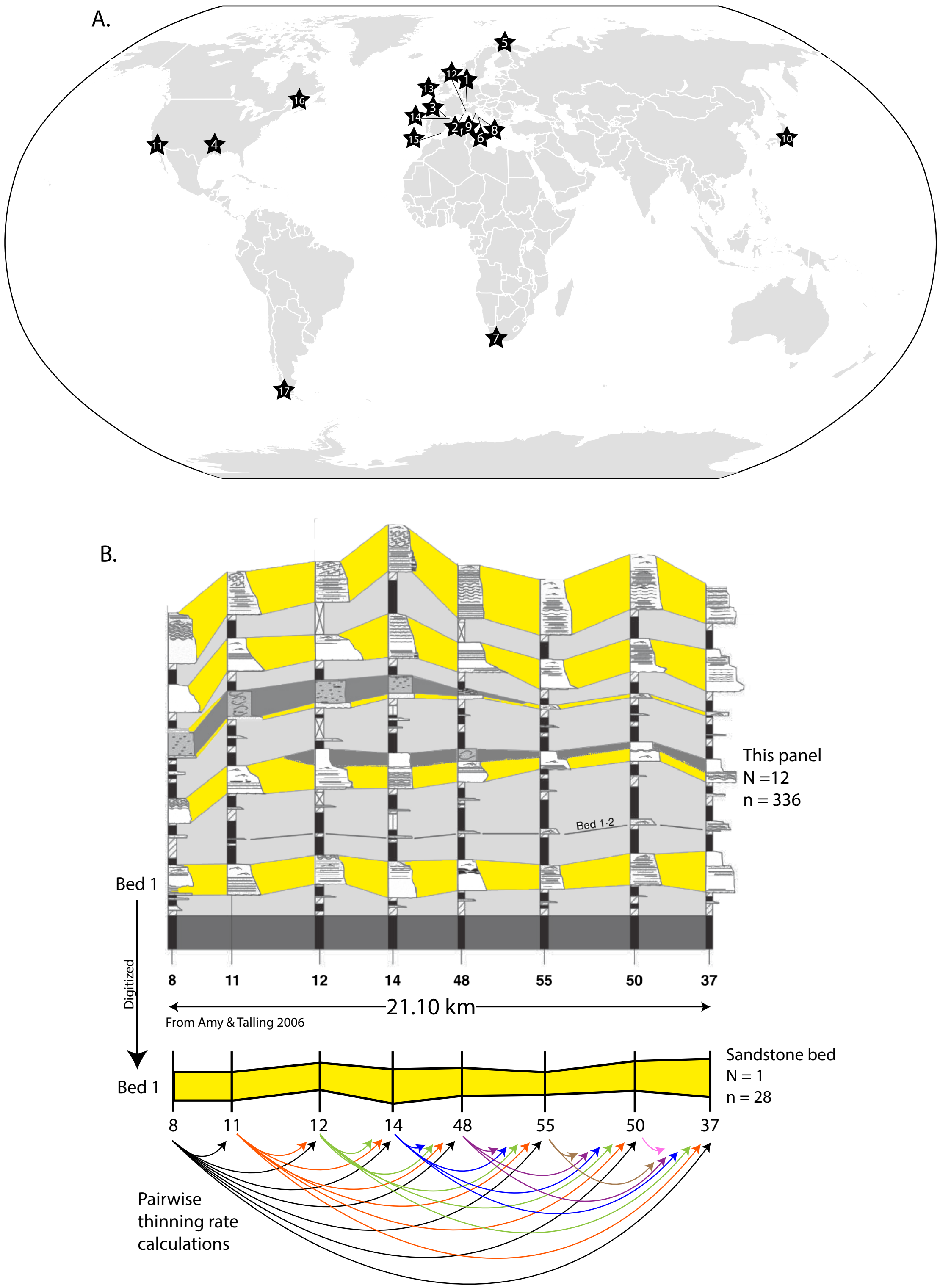

Figure 1: (A) The locations of the digitized outcrop panels. Formation, outcrop local, and reference are provided in Table 1. (B) Displays the correlation panel from Amy and Talling, 2006 with sandstone beds colored in yellow, mudstone beds colored in light grey, and debrite beds colored in dark grey. Each bed was digitized and thinning rates were calculated in a pairwise fashion (bottom). The number of beds (N =12) and the number of thinning rate values (n=336) are provided in Table 1 for each panel.

	Formation Name	Outcrop Name/Location	Environment	This Project Environment	Confinement	Paleo-curren	Distance (km)	Interval Thickne	No. of Panels	N (beds)	n (points)	Panel Reference	Interpretation
1	Cengio Turbidite System, Italy	Bormida di Millesimo valley	Base of slope lobe - medial or distal	Distal Lobe	Semi-enclosed - Base of Slope (1)	Dip	5km	30m	4	138	708	Bersezio et al 2009	
2	Gres d'Annot Formation, SE France	Montagne de Chalufy Onlap	Slope Basin - Sheet like turbidites	Lobe	"Ponded" Foreland Basin (2)	Dip	200m	15m	1	21	37	Hilton & Pickering 1995	Joseph and Lomas 2004
3	Hecho Group, Ainsa I, Pyrenees Spain	Ainsa Quarry	Channel	Channel		Dip	200m	25m	1	65	1041	Vipond 2005	
	Hecho Group, Banaston-2 Allogroup, Pyrenees, Spain	Anso to Jaca	Distal to Basin Plain Transition	Basin Plain		Dip	30km	80m	2	89	261	Remacha et al 2005	
	Hecho Group, Banaston-2 Allogroup, Pyrenees, Spain	Anso to Jaca	Basin Plain	Basin Plain		Dip	30km	80m	1	15	126	Remacha & Ferdinand 2003	
	Hecho Group, Jaca Complex, Pyrenees, Spain	RCH2b; Rapitan System near Jaca	Levee-Overbank	Levee		Dip	1km	50m	1	63	440	Remacha et al 1995	
4	Jackfork Group, Arkansas, USA	DeGray Lake Spillway	Lobe	Distal Lobe	Base of Slope (1)	Dip	90m	30m	2	124	117	Slatt et al 1997	Al-Siyabi 2000; Slatt et al. 2000; Zou 2015
5	Kongsfjord Fm., Finnmark, Norwary	East Nälneset section	CL Transition	CL Transition		Stike	150m	8m	1	60	658	Drinkwater 1995	Drinkwater & Pickering 2001
	Kongsfjord Fm., Finnmark, Norway	Hamningberg & West Nälneset	Channel	Channel		Strike	1200m	100m	2	49	2976	Pettingill et al 1993	
	Kongsfjord Fm., Finnmark, Norway	Veines - PS V1 - V2	CL Transition	CL Transition		Dip	1km	50ft	2	68	317	Pettingill et al 1993	
	Kongsfjord Fm., Finnmark, Norway	Veines - PS V3	Proximal Lobe	Proximal Lobe	Passive Margin (0)	Dip	1.2km	25ft	1	39	502	Pettingill et al 1993	
	Kongsfjord Fm., Finnmark, Norway	Veines - below PS V-1	Distal Lobe	Distal Lobe	Passive Margin (0)	Dip	400ft	60ft	1	70	180	Pettingill et al 1993	
6	Laga Formation, Italy	Mt. Bilanciere Sector	Medial to Distal basin floor	Distal Lobe	Foreland Basin with full fault bounding (2)	Strike	4km	600m	1	53	166	Bigi et al 2009	
	Laga Formation, Italy	Mt. Bilanciere Sector	Channelized proximal portion of basin	Channel		Strike	2km	200m	1	59	200	Bigi et al 2009	
7	Laingsburg Fm. Karoo Basin, South Africa	Skeiding Unit B - Channel C2	Channel to Channel Margin/Base of slope	Channel/Proximal Lobe		Stike	~8km	100m	1	11	910	Brunt et al 2013	
8	Lower Laga Formation, Italy	Mt. Bilanciere Complex	Proximal/Distal Lobe Semi-confined	Proximal/Distal Lobe	Laterally Confined Foreland Basin (1)	Strike/dip	10km	30m	3	63	275	Marini et al 2015	
	Lower Laga Formation, Italy	Crognaleto Complex	Proximal/Distal Lobe Confined	Proximal/Distal Lobe	Fully Confined Foreland Basin (2)	Stike/dip	10km	30m	3	71	385	Marini et al 2015	
9	Marnoso Arenacea Formation, Italy	Northen Apennines	Abyssal Plain	Basin Plain		Dip	120km	30m	6	131	3,345	Amy and Talling 2006	
10	Otadai Fm., Boso, Japan	Boso Peninsula	Outer fan to contourite	Distal Lobe	Forearc Basin - no confinment (0)	Strike	3.5km	10m	1	21	21	Ito 1997	
11	Point Loma Fm., California USA	Cabrillo National Monument	Distal Lobe	Distal Lobe		Strike	500m	10m	1	132	1181	This study	
12	Rocchetta Formation, NW Italy	Hairpin and Strada Sections	Proximal lobe	Proximal Lobe	Laterally restricted by basin margin (1)	Strike	100m	5m	2	96	9089	Smith 1995	Felletti 2002
13	Ross Fm., Ireland	Kilbaha Bay	Channel Lobe Transition	CL Transition		Strike	350m	14m	1	97	764	Elliot 2000	
	Ross Fm., Ireland	Center Kilbaha Bay - Middle Sands	CL Transition	CL Transition		Strike	5000ft	25ft	1	64	449	Chapin 2007B	
	Ross Fm., Ireland	Western Kilbaha Bay	CL Transition/Broad shallow channels/midfan	CL Transition		Strike	1800ft	20ft	1	85	429	Chapin 2007B	
	Ross Fm., Ireland	Upper East Kilbaha	Channel	CL Transition		Strike	600ft	20ft	1	43	106	Chapin 2007B	
	Ross Fm., Ireland	Lower West Kilcloher	Layered Sheet Sands/Outer fan fringe	Distal Lobe	Ponded (2)	Strike	4100ft	100ft	1	61	1924	Chapin 2007	Pyles 2008
	Ross Fm., Ireland	Upper West Kilcloher	Amalgamated sheet sands/mid-fan	Proximal Lobe	Ponded (2)	Strike	2000ft	100ft	1	33	72	Chapin 2007	Pyles 2008
	Ross Fm., Ireland	East Kilcloher	Incised channels cutting layered sheets/Mid-fan	CL Transition		Strike	3000ft	100ft	1	89	863	Chapin 2007	
	Ross Fm., Ireland	East Kilcloher	Layered Sheets - lobe fringe or basin plain	Distal Lobe	Ponded (2)	Strike	1000ft	30ft	1	21	103	Chapin 2007	Pyles 2008
14	Sobrarbe Fm., Pyrenees, Spain	Huesca Province: Mondot to Urriales	Slope Channel System	Channel		Strike/Dip	100m	20m	4	95	116	Silalahi 1998	
15	Sorbas Basin, SE Spain	Lucainena de las Torres	Proximal Pond fill	Proximal Lobe	Ponded (2)	Strike	4.5km	100m	2	55	405	Haughton 2001	
16	Tourelle Fm., Quebec, Canada	Gaspe Peninsula	Thin bedded sheets	Distal Lobe	Foredeep trough (1)	Dip	700ft	30ft	1	47	516	Shew 2007	Hiscott 1980; Hiscott et al. 1986
	Tourelle Fm., Quebec, Canada	Gaspe Peninsula	Sand Sheets	Proximal Lobe	Foredeep trough (1)	Dip	700ft	80ft	1	70	549	Shew 2007	Hiscott 1980; Hiscott et al. 1986
	Tourelle Fm., Quebec, Canada	Gaspe Peninsula	Channel	Channel		Dip	700ft	80ft	1	28	485	Shew 2007	Hiscott 1980; Hiscott et al. 1986
17	Tres Pasos Fm., Chilean Patagonia	Laguna Figueroa	Slope Channel System	Channel		Dip	25m	10m	1	25	41	Macauley and Hubbard 2013	

Table 1: Compilation Database references with assigned environment

deposits, we divided the total package thickness by the number of amalgamation surfaces documented within an amalgamated body, giving a representative (i.e., mean) bed thickness. The depositional environment interpreted by the original authors is highly variable and contains moderate uncertainty of the precise sub-environment, particularly within lobe deposits (Table 1; Cf. Prélat and Hodgson, 2013). To minimize this uncertainty, we categorized each panel into broad depositional environments: channel, levee, channel-lobe transition, lobe or basin plain (Table 1). Finally, while differing interpretations exist for some outcrop localities (e.g. Chalufy locality of the Gres d'Annot: Hilton & Pickering, 1995 (slope basin), Smith & Joseph, 2004 (outer basin onlap), and Joseph et al., 2012 (channelized lobe)), we used the environment from the publication that demonstrated the most evidence for their interpretation (Table 1).

Statistical Analysis – Quantitative Parameters

For statistical comparison, bed thickness and lateral distance are the two most important types of data collected in this study. In the Point Loma Formation, bed thicknesses were collected from measured sections and lateral distance was collected from map measurements and GPS locations. In the data compilation, bed thickness and lateral distance were measured from the published correlation panel. We use equation 1 to compute the thinning rate, a dimensionless number that enables comparison of bed thickness changes over a lateral distance (Deptuck et al., 2008; Marini et al., 2015; Liu et al., 2018; Tőkés and Patacci, in press). The sign (e.g., + or -) convention for thinning rate is arbitrary and depends on which direction the thinning/thickening is occurring for a given change in bed thickness. With my method, the computed thinning rate and lateral distance are associated with the first measured section's bed thickness for all future comparisons. The lateral distance was not corrected for paleocurrent direction as it created more uncertainty within the thinning rate calculation through the unknown bed thickness change across the projected distance (see Supplemental Material A). Thinning rates were acquired in pairwise fashion (Figure 1B; e.g., section 1 to 2, 1 to 3, 1 to 4, etc.) to provide a distribution of thinning rates and to decrease the sampling bias created from measured section spacing. Thinning rates were calculated for both sand and mud lithologies. A 2D kernel density estimation (KDE) is used to estimate the distribution of the two cross-plotted variables with the kernel shown as a contour map. The KDE percentage indicates the amount of the data distribution included within that contour.

$$\text{Thinning Rate (TR)} = \frac{\Delta\text{Bed Thickness (Th)}}{\text{Distance (x)}} = \frac{\text{Th}_{\text{M1B1}} - \text{Th}_{\text{M2B1}}}{\text{x}} \tag{2.1}$$

Net-to-gross ratios were calculated at measured section locations through dividing the total sandstone thickness by the total section thickness. The 'frequency of pinch-out' parameter is the number of pinch-outs between each section normalized by the lateral distance and the number of beds within that panel. For example, if a panel has 5 total sandstone bed pinch-outs over 20 beds with a lateral distance of 1 km, the frequency of pinch-outs for this panel would be 0.00025 per meter. For a given sandstone bed, this statistic would imply that there is a 2.5% probability a sandstone bed would pinch out over 100 m. This gives a pinch-out count per meter to enable comparable ratios between environments.

Results and Analysis

Lateral Event Bed Continuity Between Depositional Environments: Results

Using the compiled correlation panels (Table 1), we can investigate architectural parameters of event beds among different submarine depositional environments. Figure 2A shows the relationship between thinning rate and bed thickness (sandstone and mudstone combined) for each environment. Channel deposits show the highest bed thickness and thinning rate ranges with 10cm to 3m and 0.03 to 10 cm/m, respectively (Figure 2A). Basin-plain deposits show thick beds (10 cm to 3 m) and the lowest thinning rates (0.0001 to 0.01 cm/m). Levee deposits display moderate bed thicknesses of 10 cm to 1 m with moderate to low thinning rates of 0.001 to 0.1 cm/m (Figure 2A). Channel-lobe-transition-zone deposits show moderate to high bed thicknesses of 5 cm to 1 m with moderate to high thinning rates of 0.005 to 2.5 cm/m. Lobe deposits overall are quite similar to channel-lobe-transition-zone deposits, but display the largest range of bed thicknesses (1 cm to 1 m) and a wide range of thinning rates (0.002 to 5 cm/m; Figure 2A).

Splitting up the event bed into sandstone and mudstone beds shows that each environment displays different characteristic sandstone/mudstone thicknesses and thinning rates (Figure 2B). Based on the median values and 90% KDE contour polygons, sandstone deposits in channel environments are thicker and have larger thinning rates compared to mudstone units (Figure 2B). Levee deposits show the opposite trend with the mudstone units being thicker and thinning more rapidly than sandstone beds. It should be noted that this result is due to the broad grouping of multiple mudstone beds and thin sandstone beds within the panel and does not reflect individual mudstone beds. Channel-lobe-transition-zone deposits appear very similar to channels, but with slightly thinner beds and slightly lower thinning rates (Figure 2B). Lobe deposits show very

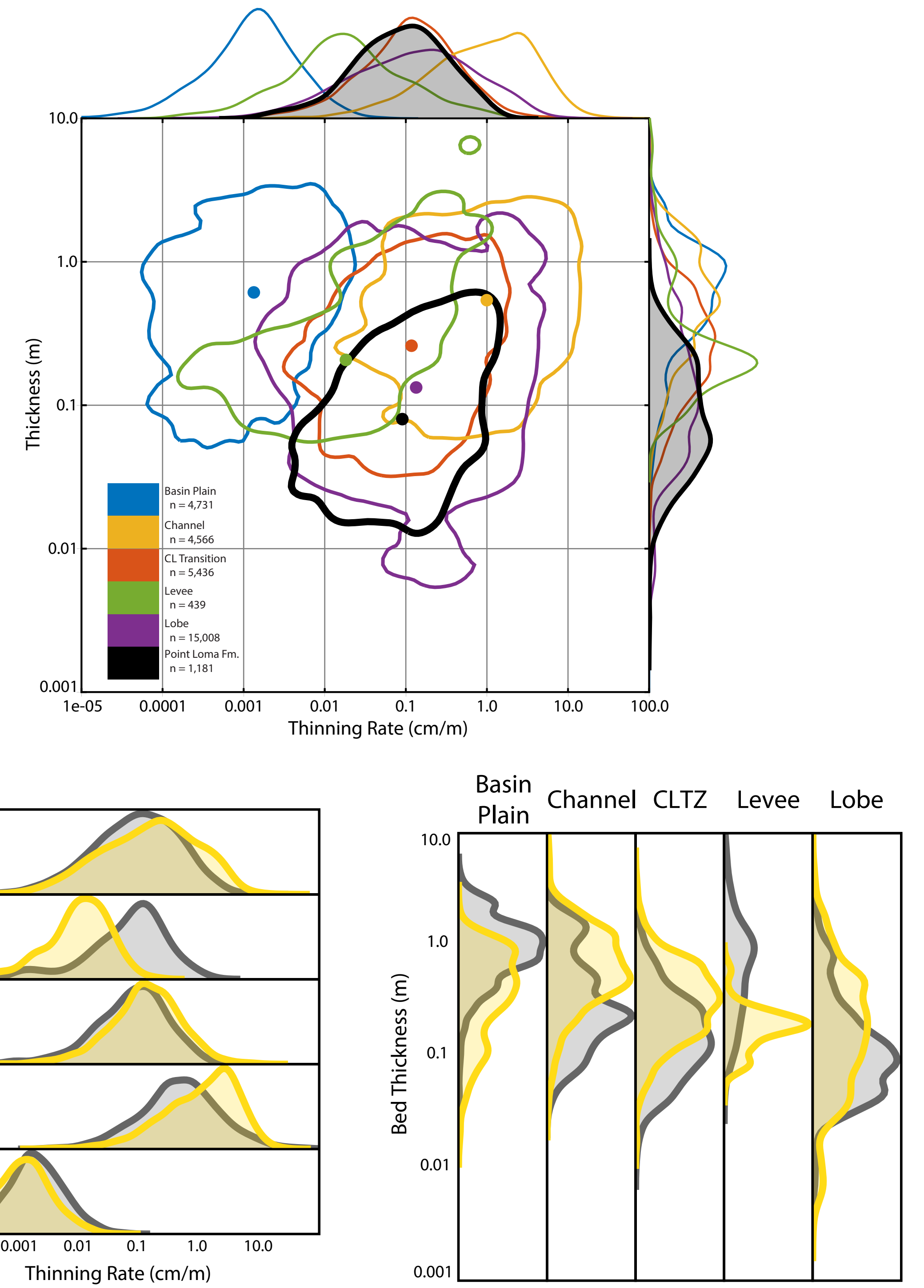

Figure 2: Thinning rates for submarine depositional environments. (A) Combined (i.e., sandstone and mudstone) plots of bed thickness and thinning rate with a 90% KDE and a median for each environment, showing that bed thickness is not a sole identifier of environment. However, applying bed thickness and thinning rate together can help identify environments. (B) The distributions of bed thickness and thinning rate plots separated by lithology. Different relationships between sandstone and mudstone in different environments likely reflects varying transport and deposition mechanisms.

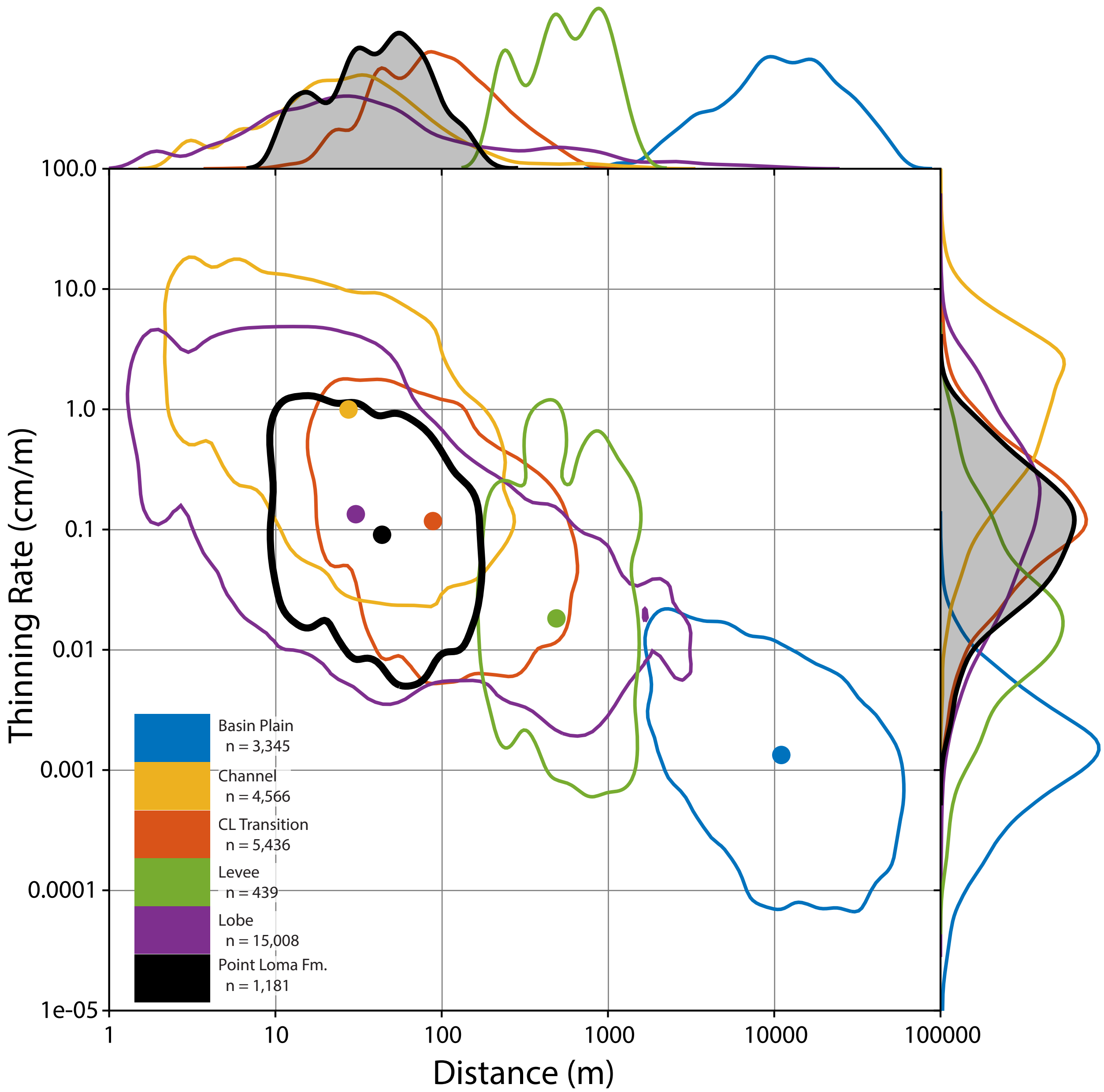

Figure 3: Lateral distance vs thinning rate with a 90% KDE and a median for each submarine depositional environment. Environments separate out by their lateral correlation distances, with channels showing the shortest correlation distance and highest thinning rates and basin plains the longest distance and lowest thinning rate. However, lobes span across all length scales, perhaps due to the degree of confinement. The vertical striping is associated with sampling bias (i.e., measured section spacing).

similar sandstone and mudstone thicknesses and thinning rates. Basin-plain deposits display higher mudstone bed thickness and thinning rates compared to sandstone beds (Figure 2B).

The lateral distance over which the thinning rate is measured (see Equation 1) is also useful to differentiate environments (Figure 3). The overall negative slope of the data in Figure 3 is intuitive and caused by distance being the denominator within the calculation for thinning rate (Equation 1). The vertical striping in Figure 3 is caused by sampling bias (i.e., the measured section spacing). Channel deposits display the highest thinning rates and the shortest bed correlation distance (1-300 m, with a median at 30 m). Channel-lobe-transition-zone deposits display moderate correlation distances from 20 to 800 m with a median at 95 m (Figure 3). Lobe deposits span the largest range of bed correlation distances of 2 m to 8 km with a median at 70 m. Levee deposits characteristically show larger correlation distances of 300 m to 1.1 km with a median at 600 m (Figure 3). Finally, basin-plain deposits show the largest characteristic correlation distances of 1.2 to 17 km with a median at 10 km.

Understanding the frequency of pinch-outs by environment is important for building stratigraphic forward models and reservoir models (e.g., Pyrcz et al., 2005). Figure 4 displays the 90th percentile frequency of pinch-outs over a lateral distance of 25 m by lithology and environment. The lowest to highest pinch-out by sandstone and mudstone lithologies is as follows: basin plain, levee, channel-lobe transition, lobe and channel deposits (Figure 4). While it appears that basin plains have no data, the 90th percentile is actually extremely close to zero. This is an intuitive result, and indicates that basin-plain deposits have the least likelihood of either lithology (sandstone or mudstone) pinching out over 25 m whereas channels display the highest likelihood of mudstone lithologies to pinch out within 25 m. A key result is that lobes display similar pinch-out rates between sandstones and mudstones (Figure 4). The 10^{th} percentile frequency of pinch-outs over 25 m for all environments is zero (i.e., all beds correlate across 25 m).

Net-to-gross is a commonly used parameter to infer depositional environments (Prather et al., 1998). The violin plots in Figure 5 show the distribution of net-to-gross values for each environment. Based on the medians, the lowest to highest characteristic net to gross environments are levee, basin-plain, lobe, channel-lobe-transition-zone, and channel deposits. However, the overlap in the distributions for channel, channel-lobe-transition-zone, and lobe deposits shows that net-to-gross alone is a very poor indicator of depositional environment. This effect is compounded by the often-arbitrary measurement of 'gross' intervals. Channel-lobe-transition-zone and basin plain deposits display the smallest variances (Figure 5). Whereas, channel deposits display the largest spread of data with the highest variance (Figure 5). Channel, channel-lobe-transition-zone and lobe deposits are skewed towards higher net-to-gross values than their means (Figure 5).

Lateral Event Bed Continuity Between Depositional Environments: Analysis

Thinning rates and bed thicknesses can be utilized for reservoir characterization to estimate reservoir extent and volume. However, based on the overlap in net-to-gross or bed thickness between each environment (Figure 2; Figure 3; Figure 5), these parameters alone are not useful to interpret depositional environment. Using a combination of bed thickness and thinning rate (Figure 2) is effective to differentiate channels, levees and basin plains (Figure 6). However, channel-lobe-transition-zone and lobe deposits display very similar bed thickness and thinning rate distributions, indicating these deposits are indistinguishable using these metrics.

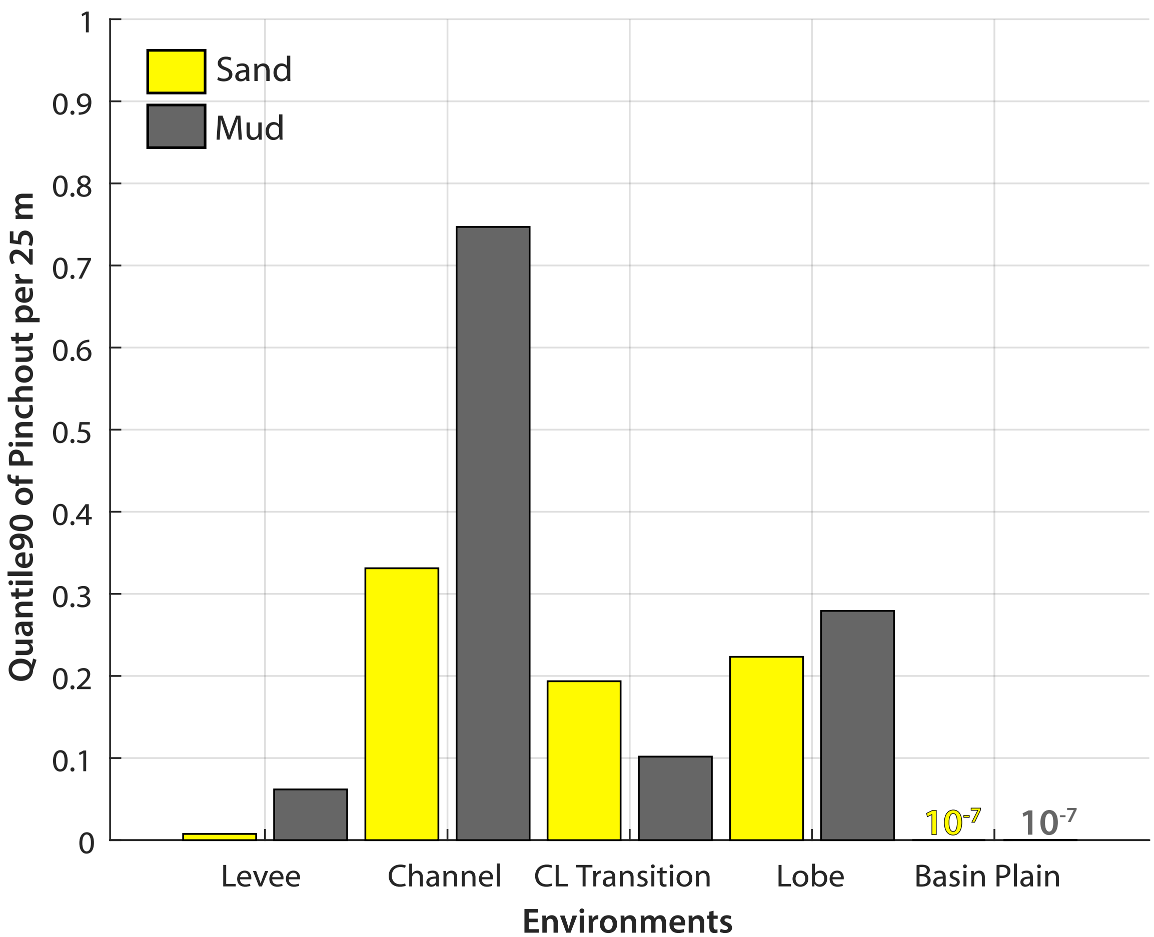

Figure 4: Environment frequency of pinch-outs by lithology per 25m. In order of increasing frequency of pinch-out: basin plain, levee, channel lobe transition, lobe, and channel.

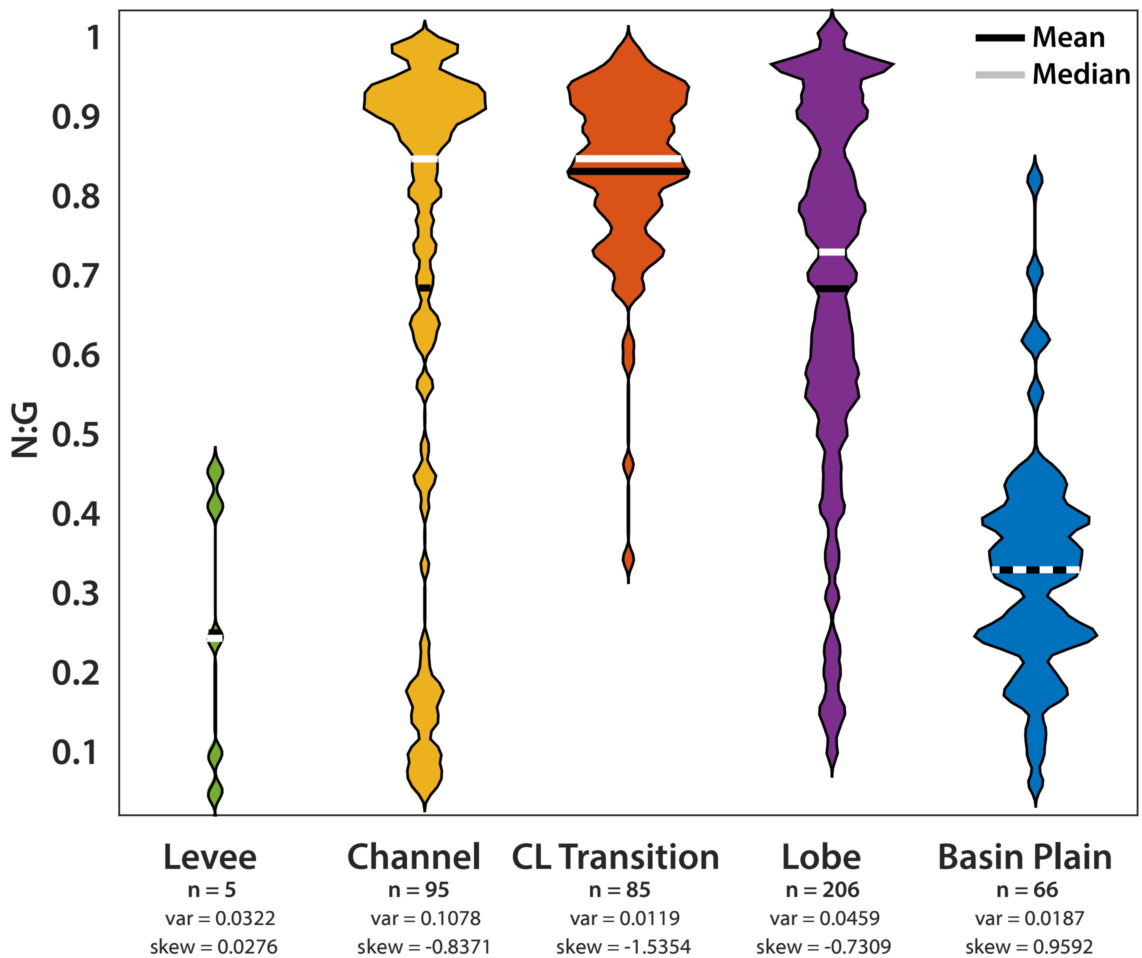

Figure 5: Environment net-to-gross distributions. In order of increasing median net-to-gross values: levee, basin plain, lobe, channel lobe transitions, and channels.

Wynn et al., (2002) document numerous erosional features in channel-lobe transition zones (CLTZ), and perhaps including a parameter that quantifies erosion (e.g., amalgamation ratio) would better differentiate CLTZ and lobe deposits.

Sandstone and mudstone lithologies display distinctive thinning rate and bed thickness relationships in different environments (Figure 2B; Figure 6) that are likely caused by their respective transport and deposition mechanisms. For example, sandstone and mudstone deposition in levee deposits is strongly influenced by flow stripping of the active channel (Piper and Normark, 1983; Peakall et al., 2000; Fildani et al., 2006). However, the sands are only deposited by flows that are suspending sand grains higher than the active levee crest, whereas muds are suspended above the levee crest during nearly every flow. Therefore, sandstone bed thickness is indicative of a single flow event, whereas the mud event bed boundaries are likely indistinguishable (Dennielou et al., 2006), producing higher characteristic mudstone bed thickness. The higher mudstone-thinning rate is due to the high degree of thin bedded sandstone beds lumping into a single mud bed, inability for complete sandstone correlation, and indistinguishable mudstone bed boundaries within the original panel creating a rapid mudstone bed thickness change and increased thinning rate. While this study only has 1 panel available for levee deposits (Table 1), the broad theoretical understanding of levee dynamics is displayed within the quantified parameters of this study (Piper and Normark, 1983; Peakall et al., 2000; Fildani et al., 2006). However, additional bed-scale correlation and quantification is needed to create a more robust dataset of levee deposits.

Channelized environments are typically the highest-energy portions of the submarine depositional system and thus display the highest amounts of erosion and bypass (Mutti and Normark, 1987; Hubbard et al., 2014; Stevenson et al., 2015). Thick sandstone beds and thinner mudstone beds, high net-to-gross, and high frequency of pinch-outs characterize the channel fill (Figure 2, Figure 4, Figure 5, Figure 6). High flow shear stresses within channelized settings leads to erosion, bypass of muddy sediment, and deposition of coarse-grained sediment (Mutti and Normark, 1987; Normark, 1989; Hiscott et al., 1997; Peakall et al., 2000; Keevil et al., 2006), creating thick sandstone beds and high net-to-gross values observed in channel deposits (Figure 2; Figure 5). Confined flow in channelized environments creates abundant erosion (Smith et al., 2005; Conway et al., 2012), producing the high pinch-out frequency of both sandstone and mudstone (Figure 4). The wide-ranging distribution of channel net-to-gross (-Figure 5) is indicative of the inclusion of axis, off-axis, and margin facies into channel-deposit correlation panels (e.g., Hubbard et al., 2014). While it is out-of-scope for this study, more detailed dissection of this facies-level data may lead to better constraints on channel-deposit architecture. The event bed correlation distance in channel deposits is less than 300 m (Figure 3) and is limited by the channel dimensions (Konsoer et al., 2013; Shumaker et al., in press).

Channel lobe transition zones (CLTZs) are characterized by the initial loss of confinement from the active channel but still contain a high degree of erosion and bypass (Mutti and Normark, 1987), which is commonly displayed as smaller channels and mega-flutes (Wynn et al., 2002; Covault et al., 2016; Carvajal et al,. 2017). The data collected from CLTZs show slightly lower bed thicknesses and thinning rates in both lithologies, longer correlation distances and lower net-to-gross as compared to channels (Figure 2 & Figure 3). The loss of confinement and decrease in shear stress allows the flow to distribute the sediment across a wider surface, reducing bed thickness and thinning rates. The narrow distribution of high net-to-gross found within the CLTZ's supports the erosion documented in these deposits (Wynn et al., 2002;

Covault et al., 2016; Carvajal et al., 2017), and suggests that mud is either being eroded here or rarely deposited (Figure 5).

In general, lobe environments are described by the total loss of channel confinement (Piper and Normark, 1983). As the flow expands, the environment becomes dominated by deposition with a distal increase in mud (e.g., Mutti and Normark, 1987; Deptuck et al., 2008). However, basin confinement can alter this facies model (discussed below; also see Jobe et al., 2017). In lobe deposits, sandstone and mudstone beds display similar thickness values, with sandstones occasionally being thicker, as shown by the net-to-gross skewed towards higher values (Figure 2 & Figure 5). However, the broad distribution of net-to-gross values (Figure 5) indicates that the compiled data sample a range of internal lobe subenvironments that have different associated parameter values (e.g. proximal/axial – high net-to-gross, medial – moderate net-to-gross, and distal/fringe positions – low net-to-gross). Lobe deposits overlap all other deposits in bed thickness, thinning rates, correlation distance, and net-to-gross (Figure 2 & Figure 3). This is likely caused by (1) the extreme facies variability in lobe deposits (e.g., Deptuck et al., 2008; Croguennec et al., 2017) and (2) differing sediment supply, basin configuration, and tectonic setting of the compiled database (Table 1). Lobes also display similar pinch-out frequencies between both lithologies indicating that the mudstones are just as continuous as sandstone beds (Figure 4).

Basin plains are characterized by very distal areas with very low gradients and long-distance correlations (Amy and Talling, 2006; Clare et al., 2014). Erosion is rare in basin-plain environments due to low shear stress (Weaver et al., 1992). A key difference between basin plain and all other deposits is their extremely large correlation distances and low thinning rate values (Figure 2 & Figure 3), which is caused by the complete loss of confinement and low gradients

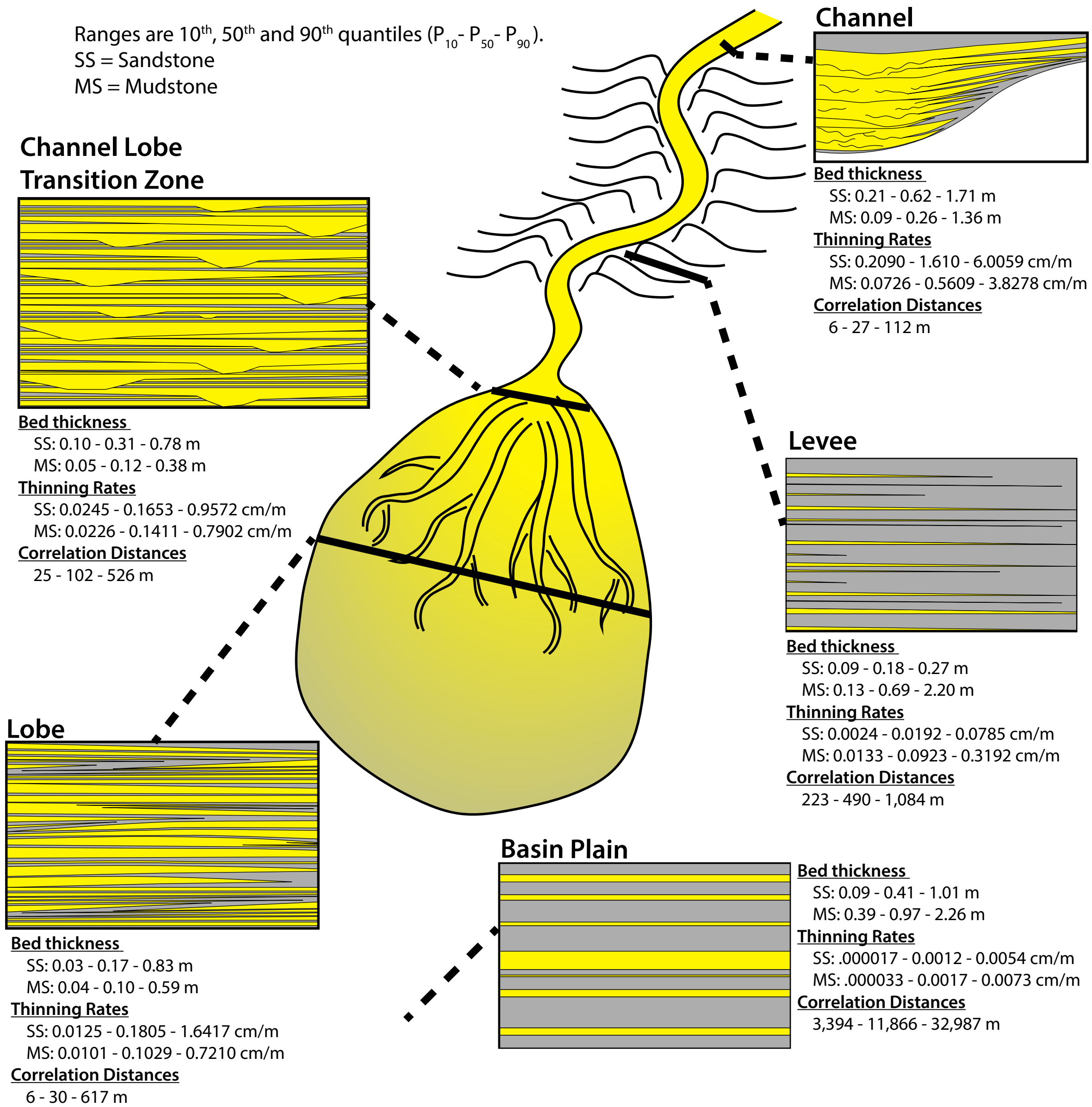

Figure 6: Summary of the results (bed thickness, thinning rates, and correlation distances) from the compilation database. Ranges listed are 10th, 50th, and 90th quantiles (P10 - P50 - P90). Sandstone = SS, Mudstone = MS.

allowing full expansion of the flow to evenly cover large areas (Weaver et al., 1992; Amy and Talling, 2006; Sumner et al., 2012; Stevenson et al., 2014). Sandstone bed thicknesses in basin plains are similar or thicker than channels, CLTZs and lobes, indicating that only very large flows are depositing sand on the basin plain (Jobe et al., 2018). However, net-to-gross is low and mudstone beds are thick, further supporting the low energy interpretation (Figure 2 & Figure 5). The high proportions of mudstone likely indicate that event frequency of sand-rich flows is low (e.g., Clare et al., 2014; Jobe et al., 2018), leading to thick mud accumulations between sand beds.

Lobe Sub-environments and Effective Confinement: Results

Submarine lobe deposits often show the most variability in event bed lateral continuity (Figure 2; Figure 3; Figure 4) and net-to-gross (Figure 5). To explore this variability, we classified lobe sub-environments to provide a more detailed analysis. We chose the following sub environments: unconfined proximal, unconfined distal, semi-confined proximal, semi-confined distal, confined proximal and confined distal. Proximal and distal lobe deposits in unconfined settings have similar mudstone bed thicknesses, but proximal lobes have thicker sands compared to their distal counterparts (Figure 7). However, unconfined distal lobe deposits display lower thinning rates than unconfined proximal lobes (Figure 7). The semi-confined setting shows that their proximal deposits have thinner sandstone and mudstone beds but thin at a similar rate when compared to their distal areas (Figure 7). Lastly, confined proximal lobe deposits display higher sandstone and mudstone thickness but with similar thinning rates compared to confined distal lobe deposits (Figure 7). Out of all lobe sub-environments, confined proximal lobe deposits display the thickest sandstone and mudstone beds and the lowest thinning rates (Figure 7), similar to many confined Gulf of Mexico minibasins (e.g., Prather et al., 2012).

The net-to-gross values for the lobe sub-environments are broadly similar, but important differences exist (Figure 8). Based on the median values, net-to-gross is lower for the distal settings of unconfined and semi-confined lobes compared to their proximal counterparts (Figure 8), validating classic facies models for lobes (e.g., Normark, 1978; Deptuck et al., 2008; Prélat et al., 2009). However, confined lobes show the opposite trend, with proximal confined lobe deposits showing a range of net-to-gross values, but distal confined lobe deposits showing high net-to-gross values (Figure 8). Whereas these trends in net-to-gross are interesting and validate previous models, we urge caution in relying solely on these distributions, as they are likely incomplete due to small sample sizes (in particular for unconfined proximal/distal and confined proximal).

Lobe Sub-environments and Effective Confinement: Analysis

Confined and unconfined lobe deposits have very different planform shapes (Prélat et al., 2010; Pettinga et al., in review) and sandstone/mudstone bed thickness distributions (Marini et al., 2015). An unconfined lobe was defined as an incoming flow that had no lateral or distal topographic barriers, which allows for the flow to fully expand and for the mud fraction to be transported to the most distal reaches of the lobe regardless of basin shape or size (Damuth and Flood, 1983; Picot et al., 2016). In contrast, semiconfined and confined lobes have differing spatial distributions of sandstone and mudstone due to the presence of topographic barriers (e.g., Prather et al., 1998). A semiconfined system would allow for the mud fraction of the flow to bypass, but the sand to be deposited or bypassed (Prather et al., 1998; Jobe et al., 2017). On the other hand, a fully confined system has flows that cannot fully expand within the basin and would prevent the sand and mud fractions from exiting the basin (Prather et al., 1998; Lamb et al., 2006; Pirmez et al., 2012; Prather et al., 2012; Sylvester et al., 2015).

The data confirm that confined lobes have thicker sandstone and mudstone beds and lower net-to-gross values as compared to unconfined and semiconfined lobes (Figure 7; Figure 8). The plots also show that the distal portion of all confinement ratings thins at a lower rate, indicating a more tabular geometry. This result is due to the decreasing energy and shear stress in the more distal reaches of lobe environments or the degree of effective confinement is quite low (Figure 3). However, if the distal pinch-out is documented, there should be higher thinning rates there (but just at that point), and this likely does not affect bulk statistics. Both sandstone and mudstone bed thickness decrease from confined to unconfined to semiconfined lobes (Figure 7). This relationship is expected for confined to unconfined and confined to semiconfined as the flow within a confined system is unable to laterally expand, creating an overall thicker characteristic bed (Prélat et al., 2010; Marini et al., 2015; 2016). However, the lower bed thickness results for proximal semi-confined compared to proximal-unconfined lobe deposits is counterintuitive, and may represent the higher degree of bypass for the proximal portion of semiconfined lobe deposits, creating a lower characteristic bed thickness (Figure 7) (Prather et al., 1998; Jobe et al., 2017). The deposits have comparable distal bed thicknesses due to similar mechanisms of deposition (decreasing energy and shear stress) (Figure 7) (Mutti and Normark, 1987).

Depositional models and outcrop studies for submarine lobe deposition generally display a decreasing sand content, amalgamation, and bed thickness from axis to margin/fringe (Walker & Mutti, 1973; Ricci-Lucchi, 1975; Shanmugam & Moiola, 1988; Sullivan et al., 2000; Deptuck et al., 2008; Jegou et al., 2008; Prelat et al., 2009; Groenenberg et al., 2010; Etienne et al., 2012; Spychala et al., 2015; Fonnesu et al., 2017). My results confirm that sandstone bed thickness decreases and mudstone content increases from proximal to distal for unconfined and confined lobes (Figure 7). However, semiconfined lobes display thicker sandstones and mudstones with an increasing mud proportion within their distal reaches possibly indicating a higher degree of bypass in the proximal location (Figure 7). While these relationships could differ due to a number of basin specific parameters (e.g. basin geometry, grain size distribution, degree of confinement/bypass) or a sampling bias in the data collection or that the original interpretations are not objectively done, my data confirm these depositional models and provides important quantitative constraints on event bed parameters. However, the results for semiconfined lobes indicate that the degree of lobe confinement and subenvironment is not easily interpretable at the outcrop scale unless there is direct spatial evidence (Prélat and Hodgson 2013; Marini et al., 2015).

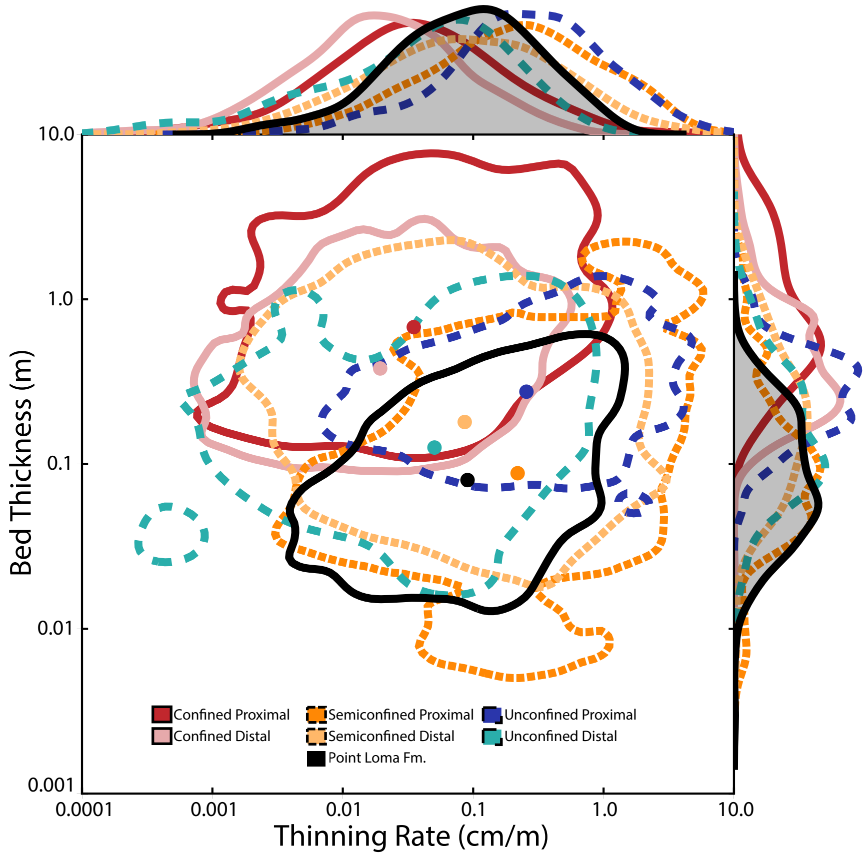

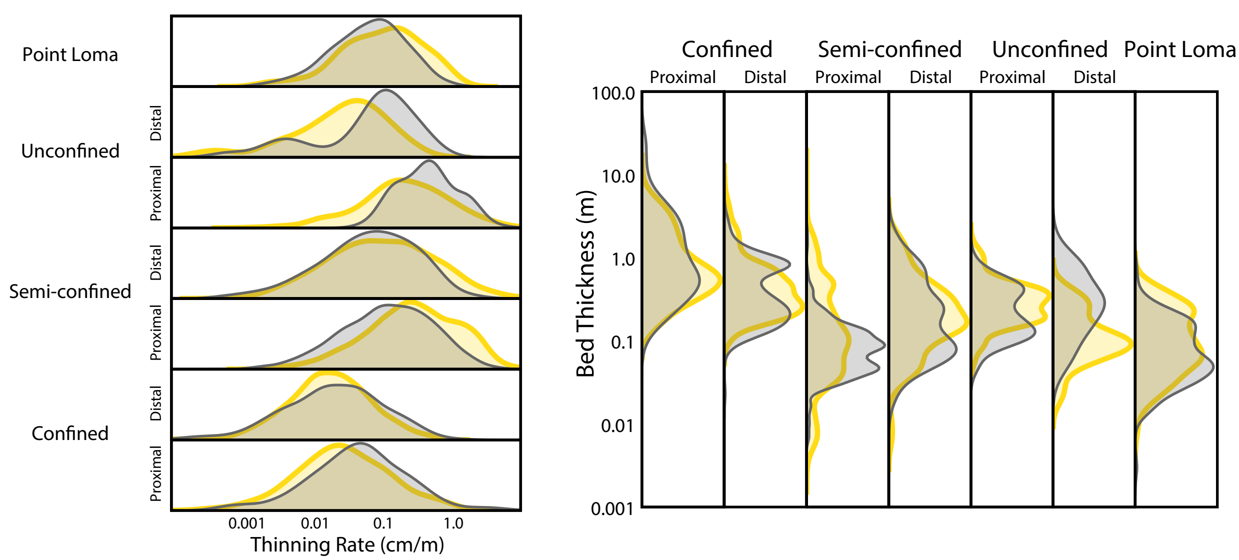

Figure 7: (Top) Lobe confinement and subenvironment plots containing bed thickness (m) and thinning rate (cm/m) of both lithologies with 80% KDE contours and median. (Bottom) Lobe confinement and subenvironment split by lithology. Generally, confined lobes show thicker beds with lower thinning rates. Unconfined lobes show moderate bed thickness and thinning rates. Semiconfined lobes show the lowest bed thicknesses and highest thinning rates. Confined and unconfined show decreasing bed thicknesses from proximal to distal while semiconfined lobes do not.

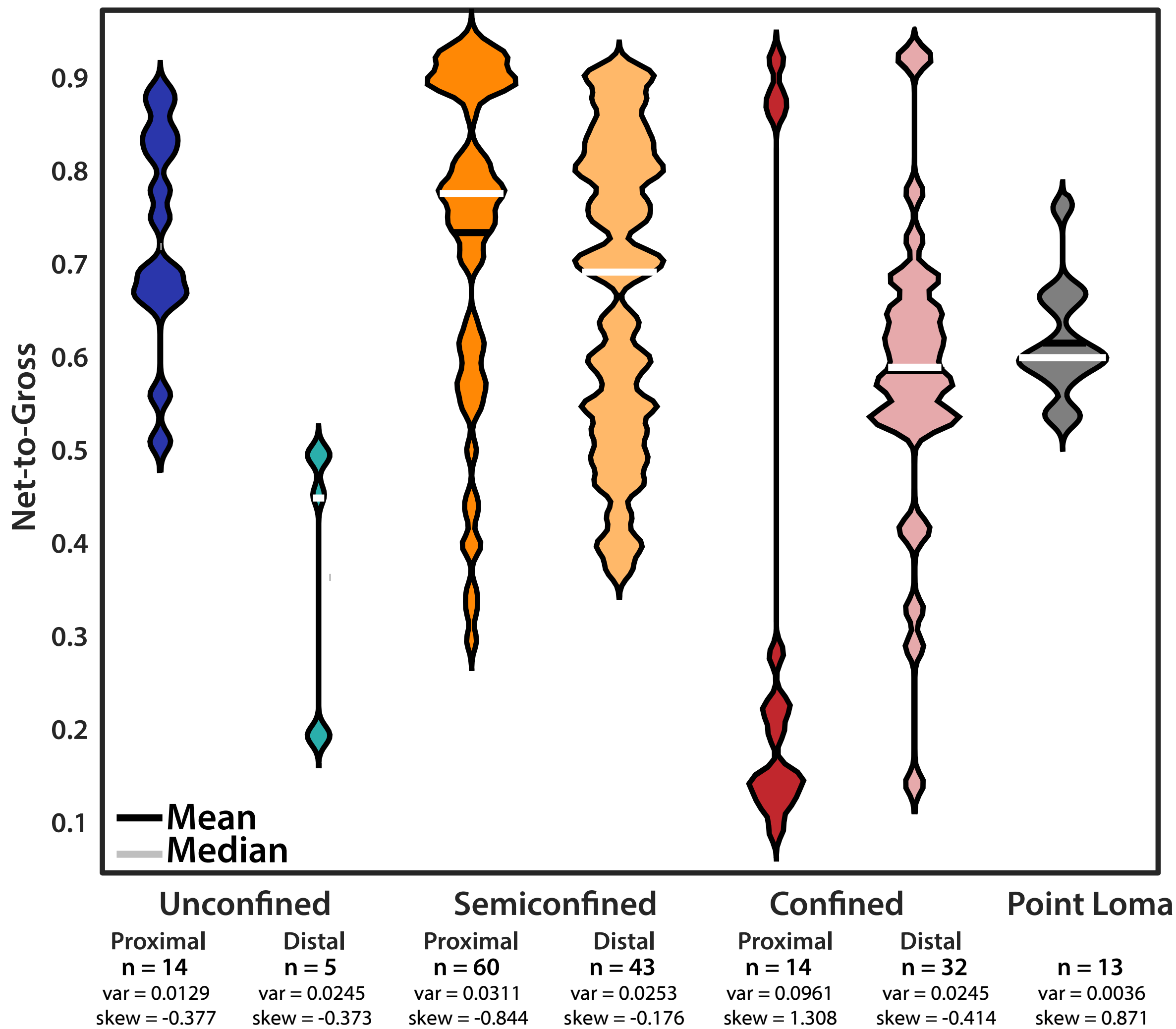

Figure 8: Lobe net-to-gross by subenvironment and degree of confinement. Unconfined and semiconfined lobes display decreaseing net-to-gross from proximal to distal. Confined lobes display a split in proximal net-to-gross values and a tight, moderate net-to-gross distribution for their distal subenvironment. Point Loma Fm. shows a tight distribution (low variance) between 0.5 and 0.75.

Application to the Point Loma Formation

To apply the results and learnings from the compilation study above, the submarine lobe strata of the Upper Cretaceous Point Loma Formation at Cabrillo National Monument near San Diego, California were selected as it has great exposure and some ambiguity in the interpreted depositional environment.

GEOLOGIC BACKGROUND

During the Late Cretaceous, the Rosario Group (Figure 9A) was deposited in a forearc basin setting caused by subduction of the Farallon plate beneath the North America plate (Atwater, 1970). Conversion of Southern California to a strike-slip setting has resulted in extensive Cenozoic strike-slip deformation (Figure 9B). The Rosario Group is intermittently exposed as coastal outcrops along southern California and Baja California’s eastern coast (Popenoe 1973; Morris et al., 1989; Morris and Busby-Spera, 1990).

At the base of the Rosario Group is the nonmarine, conglomeratic Lusardi Formation (Figure 9A), which is exposed north of San Diego and onlaps the pre-Turonian Santiago Peak Formation (Nordstrom 1970; Peterson 1970; Nilsen and Abbott 1981). The Point Loma Formation, which unconformably overlies the Lusardi Formation, is interpreted as submarine lobe deposits and slope to basin-floor mudstones (Figure 9) (Nilsen and Abbott 1981). Overlying the Point Loma Formation, sandstones and conglomerates of the Cabrillo Formation have been interpreted as coarse-grained inner to middle submarine fan deposits (Figure 9) (Nilsen and Abbott 1981), and are likely conglomeratic submarine channel deposits (cf. Jobe et al., 2010). Eocene sandstones and conglomerates above the Cabrillo Formation are marked by an erosional unconformity at the base and grade from shallow-marine into a submarine-canyon complex (Figure 9) (Kennedy 1975; May et al., 1991, May & Warme 1991). The Eocene formations are exposed northward of the La Jolla peninsula and have been extensively studied (Figure 9) (Peterson 1970; Kennedy & Moore 1971; Kennedy 1975; May et al.,1991; May & Warme 1991; May & Warme 2007; Stright et al.,2014; Ono 2017).

During the Campanian-Maastrichtian periods (84-66 Ma), the Point Loma Formation was deposited in a deep-marine forearc basin setting, likely with relatively steep slope gradients (Nilsen and Abbott 1981). It was sourced from the Peninsular Ranges from the east and paleoflow measurements indicate a west-northwest transport direction (Girty, 1987; Nilsen and Abbott, 1981; Fleming 2010). The Point Loma Formation experienced ~550 km of translation (~ 550 km) and ~40 degrees of rotation, similar to its source, the Cretaceous Peninsular Ranges batholith (Marshall and McNaboe, 1984). However, the Point Loma Formation is exposed west of the Pleistocene right-lateral strike-slip Rose Canyon Fault zone, which has an unknown displacement (Moore and Kennedy, 1971; Kennedy, 1975).

The Point Loma Formation is divided into three units: Unit 1 is a shallow marine sandstone, Unit 2 is dominated by slope mudstones and thin-bedded submarine fan deposits, and Unit 3 is dominantly thick-bedded submarine fan and channel deposits (Figure 9A) (Sliter, 1979; Nilsen and Abbott, 1981; Yeo, 1982). Using foraminiferal faunal assemblages, the outer-fan sandstone deposits of Unit 2 are interpreted to have a paleobathymetric depth of 850-1000 m whereas the middle fan sandstone deposits of Unit 3 are interpreted to have paleobathymetric depths of 600-700 m (Figure 9) (Sliter, 1979; 1984; Nilsen and Abbott, 1981). Within Units 2 and 3, Fleming (2010) documents four lobe complexes that compensationally stack and display a systematic proximal-to-distal decrease in thickness in vertically amalgamated sandstone ratio, net-to-gross, and erosion. Within a single lobe element that lies within complex two of Fleming (2010), Stammer (2014) documented in an axis-to-margin transect an increase in mud content, organic matter and mud clasts with mineralogical increases in K-feldspar, plagioclase, and biotite. This work highlighted the transition from axis-to-margin in sediment transport mechanisms, style of deposition, and hydrodynamic fractionation (Stammer, 2014).

The deposits of the Point Loma Formation within the Cabrillo National Monument (Figure 9B) are the focus of this portion of the study and are contained within Unit 2 of Nilsen and Abbott 1981 and Lobe Complex 3 of Fleming (2010). Seacliff exposures contain thin (<20 cm), laterally extensive, interbedded sandstone- and siltstones with a modal paleocurrent of 294^0 (n = 167) (Figure 9B; Sliter, 1979; Nilsen and Abbott, 1981; Fleming, 2010; this study). While we did not adjust the panel for paleocurrent, the panel obtain would have been adjusted to a strike orientation and would theoretically have higher thinning rates than a comparative dip panel orientation. The Cabrillo National Monument area is interpreted by Fleming (2010) to represent four lobe elements within the distal part of Complex 3 (Fleming, 2010). However, rapid lateral thickness changes occur at the bed-scale (Figure 10), which is not typical of distal lobe models but has been document in other recent outcrop studies (Walker & Mutti, 1973; Ricci-Lucchi, 1975; Shanmugam & Moiola, 1988; Lien et al., 2003; Prélat et al., 2009; Groenenberg et al., 2010; Etienne et al., 2012; Spychala et al., 2015; Fonnesu et al., 2016; 2017).

Field Data Collection Methodology

This study characterizes the Point Loma Formation deposits using centimeter-scale measured sections, bed and bedset correlations, paleocurrent analysis, and measurements derived from a photogrammetry-based 3D outcrop model (Figure 10). Approximately 40 sandstone-mudstone couplets were correlated between 13 measured sections (Figure 11). Because we measured and correlated every event bed, we did not define traditional lithofacies (sensu Ghosh and Lowe, 1993; see review in Hubbard et al., 2008). Care was taken to identify and separate event beds,

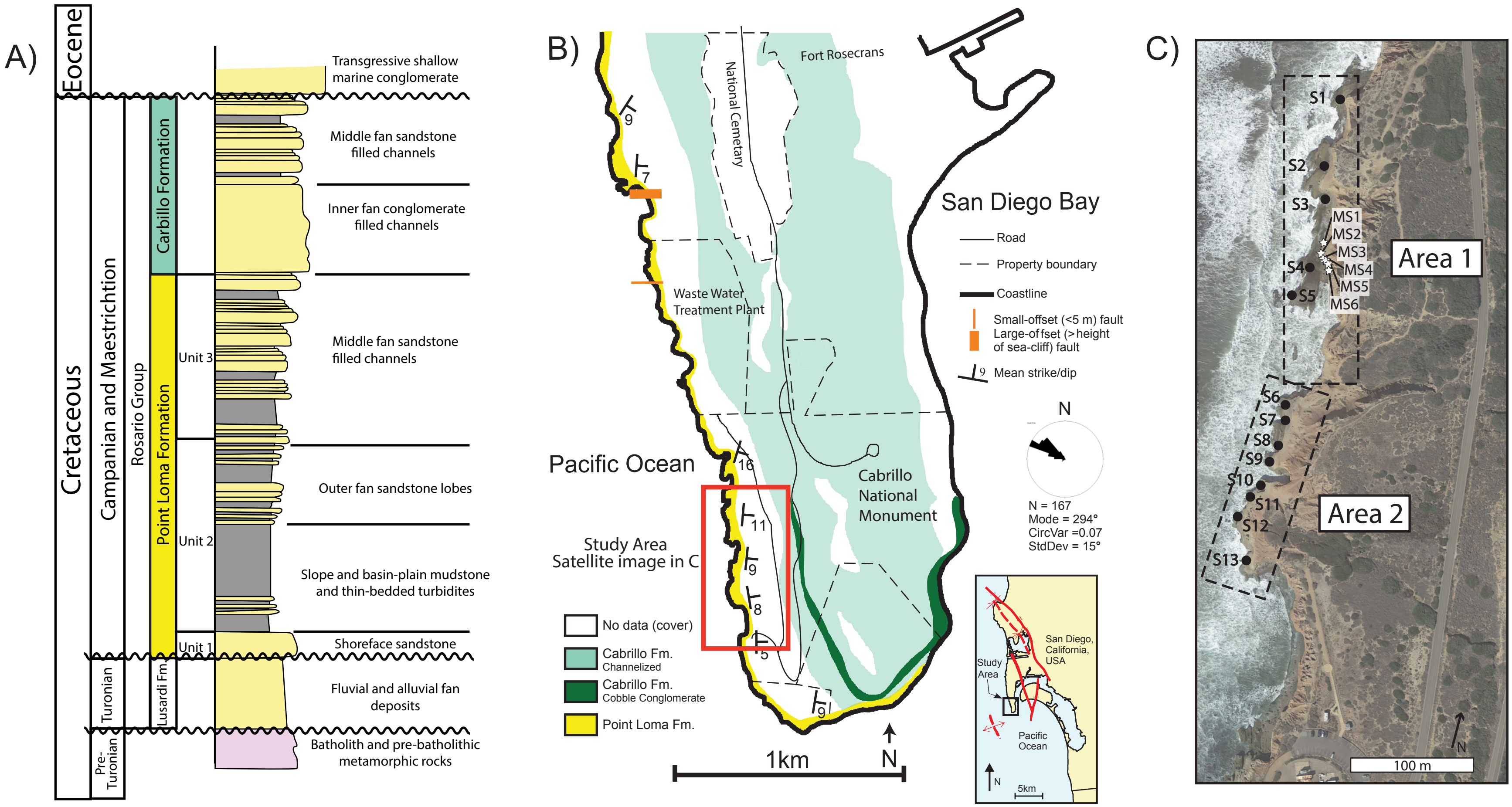

Figure 9: (A) Stratigraphic column modified from Nilsen and Abbott, 1971. (B) Map of study area on the Point Loma Peninsula in San Diego, California (modified from Fleming, 2010). Map Modified after Moore and Kennedy, 1971; USGS Topographic Map 1:24,000; and the geologic map of San Diego 30'x60' quadrangle, California (Kennedy and Tan, 2005). (C) Satellite image of Cabrillo National Monument (location shown in part B), which is subdivided into Area 1 and Area 2. Black dots are measured section locations.

the deposit from one turbidity current (Bouma, 1962; Lowe, 1982). Generally, event beds in the Point Loma Formation consist of a sandstone-mudstone couplet with Bouma-type structures (e.g., T_{abcde}; See Supplemental Material B). However, sometimes event beds are amalgamated into one sandstone bed-set; these bed-sets show flame structures and grain size changes at the event bed boundaries (see Supplemental Material B). Only one hybrid event bed (Bed “L” in subsequent figures) was identified (sensu Haughton et al., 2009), and no true debrites were measured, although they are present in the Point Loma Formation (Fleming, 2010).

The coastal exposure is divided into two areas – Area 1 to the north and Area 2 to the south – due to accessibility and a large cove in between the two areas preventing exact correlation of the lower interval (Figure 9 & Figure 10). Bed pinch-out locations were mapped and measured on photos and the 3D outcrop model (Figure 10). Lobe elements were determined qualitatively through grouping beds with similar stratal architecture and composition (Figure 10). We used major stratal surfaces and qualitative stacking patterns to interpret lobe-element boundaries (Figure 10 & Figure 11). We measured paleocurrent indicators at measured section locations (Figure 11), including parting lineations (n = 60), ripples (n= 8), flame top directions (n = 2) and megaflutes (n = 1). The mean circular paleocurrent obtained of 304^{0} (circular variance of 4.95^{0}) corresponds with the mean paleocurrent of 294^{0} (n = 167, circular variance of 0.07^{0}) collected further north along the peninsula (Figure 9B; Fleming, 2010). ‘Fining rates’ were also computed in the same fashion as equation 1, substituting grain size for bed thickness. The fining rate is the rate of lateral change of grain size within one bed. Fining rates were calculated using a mean and a maximum grain size identified by hand lens.

Classification of Lobe Elements

While multiple lobe hierarchy schemes have been developed, this study follows the hierarchy formed by Deptuck et al., (2008) and Prélat et al., (2009). This hierarchy consists of four levels: ‘beds’ deposited by an individual event/turbidity current; ‘lobe elements’ composed of stacked beds/bed sets; ‘lobes’ formed by one or more stacked lobe elements fed by a single channel; and ‘lobe complexes’ that develop when avulsions or significant channel migrations result in development of multiple lobes (Prélat et al., 2009). Due to the nature of the outcrop exposure, the Point Loma Formation allows for laterally extensive characterization of bed-scale facies and thickness variations (Figure 10). This study focuses on qualitative and quantitative identification of beds and bed-sets grouped into lobe elements through similarity in stratal architecture (e.g. bed geometries) and vertical compositional changes (Figure 10; Figure 11; Figure 12). The boundary between Elements One and Two is marked by a sharp surface characterized by the onlapping of Element Two onto Element One. The boundary between Element Two and Three is used as a datum for correlations (pink bed in Figure 11), because the boundary is a bed that is laterally continuous across the whole exposure, contains high amounts of coarse-grained biotite compared to all surrounding beds, and is paired with a mudstone that contains abundant calcite veins (Figure 10; Figure 11; Figure 12). Above this datum, Element Three thins towards the south and the sandstone beds display pinch-and-swell morphology (Figure 10; Figure 11; Figure 13). The boundary between Element Three and Four is marked by a change in architectural style with a hybrid event bed deposit at the boundary (Figure 10; Figure 11; Figure 12; Bed L in Figure 13). Element Four contains rhythmic sandstone-mudstone couplets of very similar thickness that change minimally across the outcrop (Figure 10; Figure

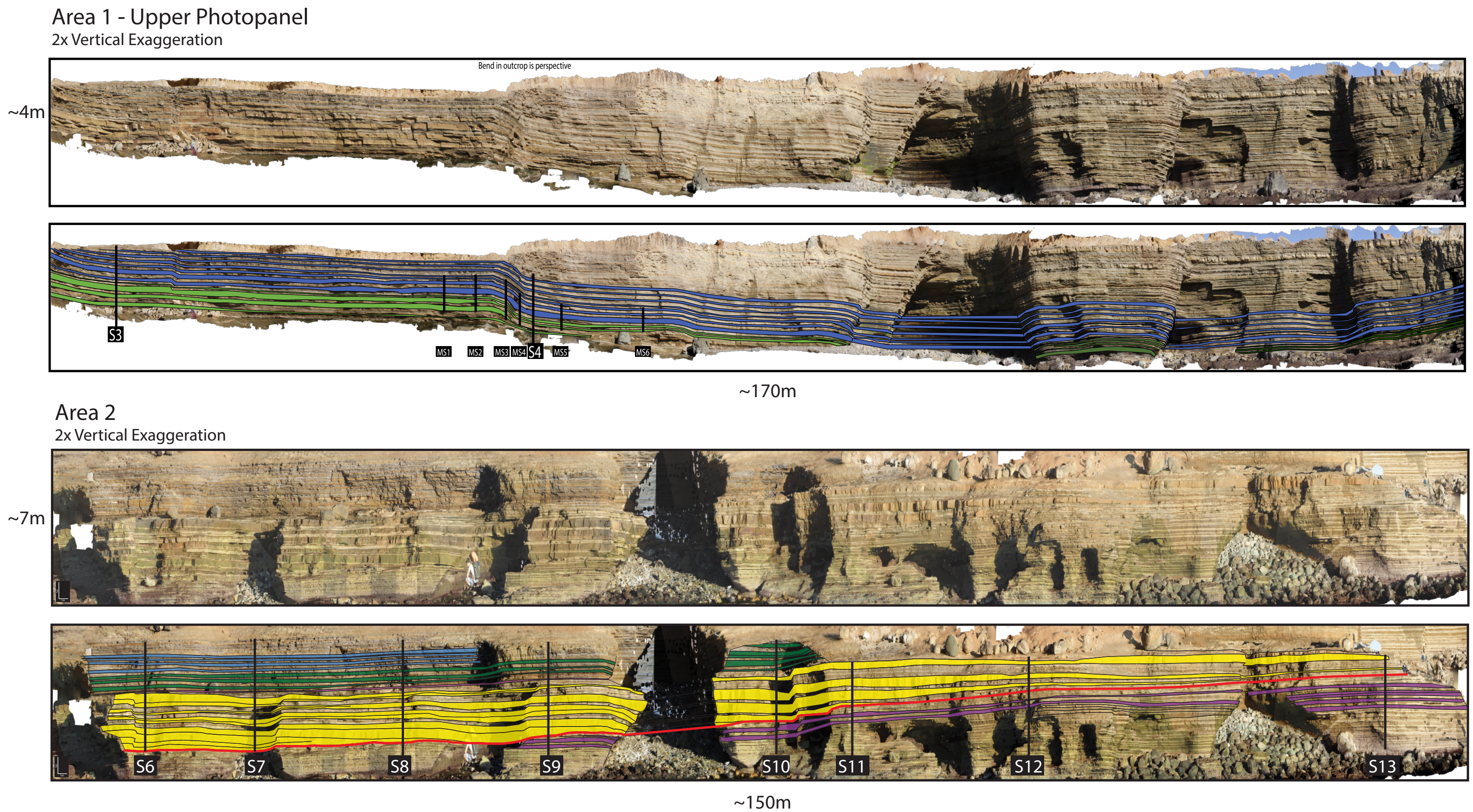

Figure 10: Digital outcrop models from area 1 (top) and area 2 (bottom) of the Cabrillo National Monument. Area 1 outcrop model is only the upper bench as indicated by the corresponding colors to figure 3. Area 2 displays onlapping geometry between the purple and yellow highlighted elements. Area 1 blue and green interval corresponds with the blue and green interval of area 2.

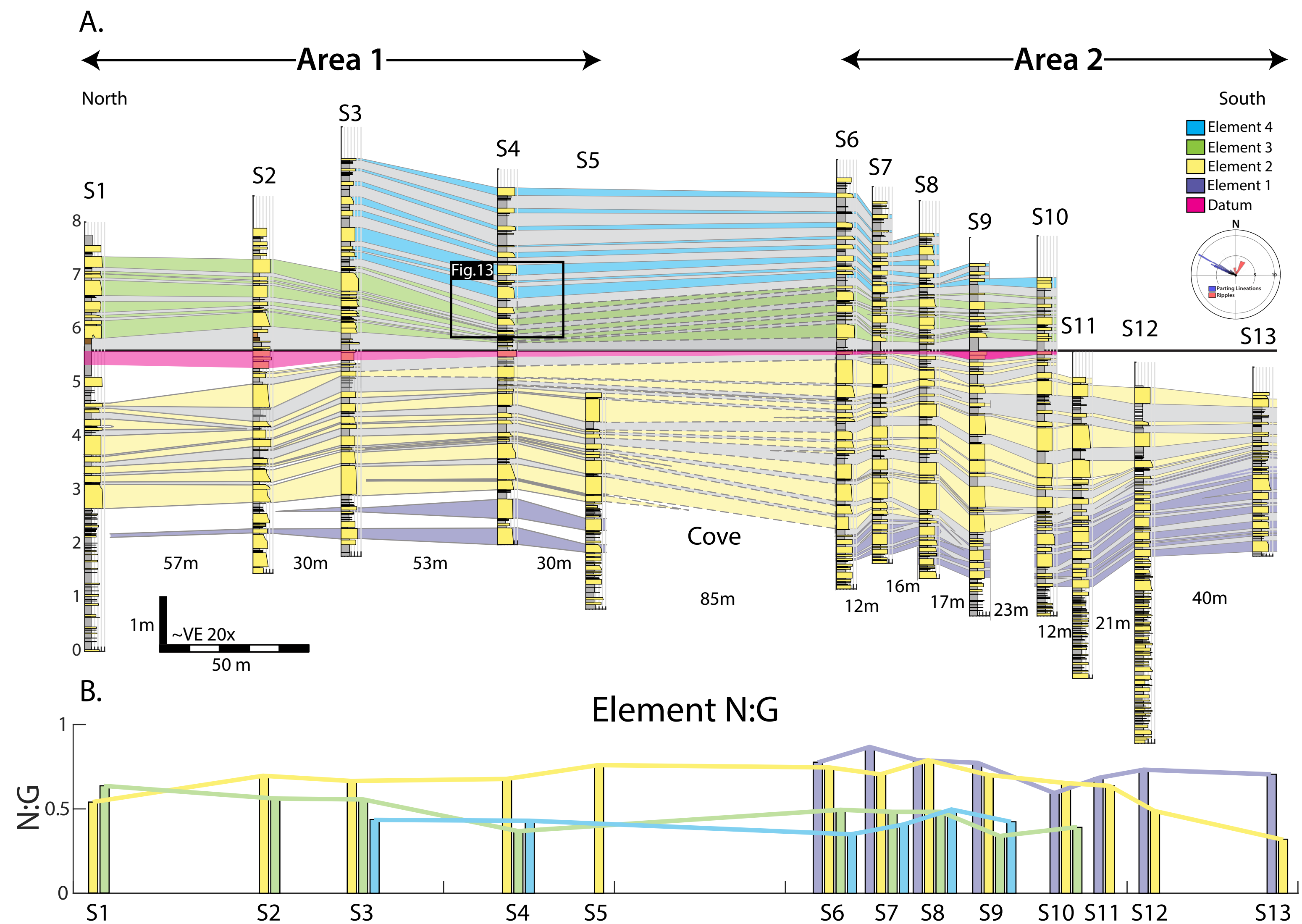

Figure 11: (A) Correlation panel of the study area (see Fig 1, 2 for location). Note the abrupt thinning and onlap of Element 2 (yellow) from north to south, whereas other elements are more laterally continuous. (B) Net-to-gross variability among lobe elements. Element 2 displays decreasing net-to-gross values in both directions from S8, whereas other elements show constant net-to-gross values (e.g., Elements 1, 4) or more complicated lateral trends (e.g., Element 3).

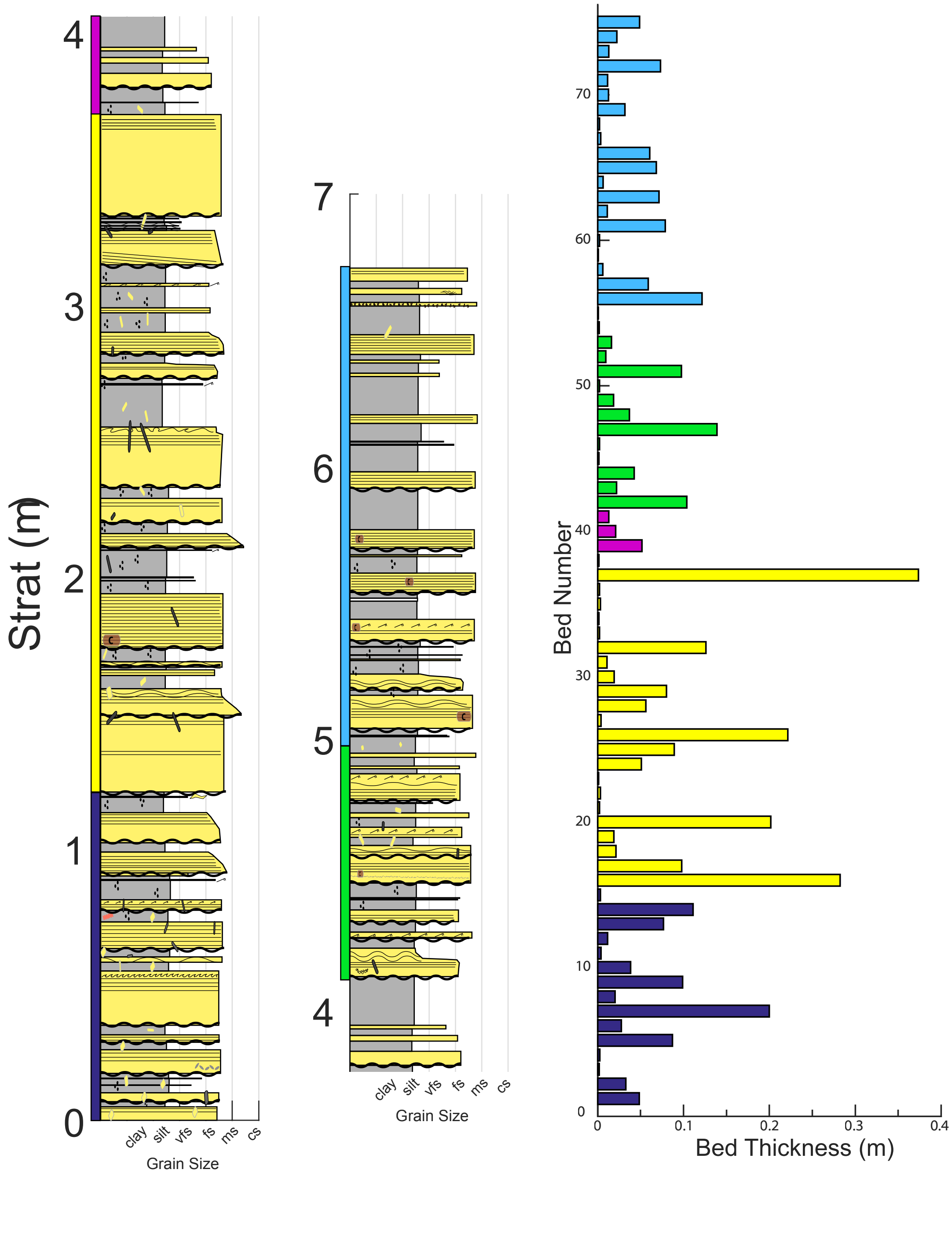

Figure 12: Measured section 6 bed thickness with associated bed number. This displays that 1D (i.e., vertical) bed thickness patterns are not diagnostic for determining lobe-element boundaries; the second dimension (i.e., lateral continuity, see Fig. 2) is needed.

11; Figure 12). Element One and Four do not display true element thickness due to base of exposure and top-truncation by Quaternary alluvial deposits, respectively.

Intra-Lobe Element Bed Architecture: Results

Within Element Three (green in Figure 13) in Area 1, subtle compensation is documented at the event bed scale (Figure 13). The basal bed (J) consistently thins southward towards MS5 with a thinning rate of approximately 0.4 cm/m then slightly thickens south of MS5. The subsequent bed (J2) thickens where J thins (between MS1 and MS2; Figure 13), and bed J3 shows more complex thickness variations. The next thick bed, Bed K, shows a similar initial thinning trend as basal bed J but thickens directly above J's most rapid thinning. Bed K also thins and thickens between S3 to MS6 in an opposite pattern to the bed directly below (J3). K2 thickens above where J and K thinned, thus showing bed-scale compensation. Hybrid event bed (L) is deposited above K2 and shows drastic thickness changes with thinning rates ranging between -0.4 to 0.55 cm/m, concurrent with a change from a sandstone-dominated to a mud-dominated lithology (Figure 13). However, bed L shows no compensation to the bed below. Bed L2 slightly thickens at MS5 above where L thins. However, L2 displays minimal thickness variation across the 25 meters with thinning rates nearing 0 cm/m. Bed M shows similar thickness trends as bed L, but the amplitude of thinning is significantly lower (Figure 13).

Event beds within Element Two (yellow in Figure 14) show two thinning trends: (1) a large-scale southward thinning and onlap/pinch-out onto Element One (purple in Figure 14; discussed below), and (2) a bed-scale compensation trend (Figure 14). The event beds thicker than 10 cm in Element Two are most affected by this compensation. For example, bed A rapidly thins southward, with thinning rates greater than 0.5 cm/m, and Bed B is thickest (50 cm) directly above the rapid thinning of Bed A (Figure 14). The next two beds are very thin (~ 3 cm) and display almost no variation in thickness. However, the next thick bed, Bed C, shows compensation with Bed B: as B thickens into S8, the overlying bed C thins (Figure 14). Then, as B thins southward from S8, C thickens to its highest recorded value (39 cm; Figure 14). The thin bed above C displays very minor thickness changes and the next bed (just below Bed D) displays a similar thickness trend to C (Figure 14). Beds D and E show the same thickness pattern from S6 to S13 with both of their highest thicknesses is where bed C is rapidly thinning. Bed F again shows its thickest portion directly above where beds D and E thin most (Figure 14). Bed F shows a similar pattern, but a lower magnitude of thinning rate compared to beds A-E. Finally, Bed G thins towards where Bed F is thickest Figure 14). This pattern is consistent and occurs throughout the element within beds greater than 10cm (e.g., beds A, B, C, D, E, F, G in Figure 14).

Intra-Lobe Element Bed Architecture: Analysis

Compensational stacking is the tendency to for a deposit to preferentially fill topographic lows, with the magnitude of compensation typically decreasing from proximal-distal (Mutti and Sonnino, 1981; Sullivan et al., 2000; Cantelli et al., 2011; Fernandez et al., 2014). There have been two proposed methods, fractal and hierarchical, for compensational stacking, which depend on either consistent compensation or variable compensation at the different hierarchical scales, respectively (Mutti and Sonnino, 1981; Mutti and Normark, 1987; Deptuck et al., 2008; Prélat et al., 2009; Straub and Pyles, 2012).

Bed compensation internal to a lobe element (Figure 13) demonstrates that turbidity currents depositing successive events react to the subtle seafloor topography created by the previous

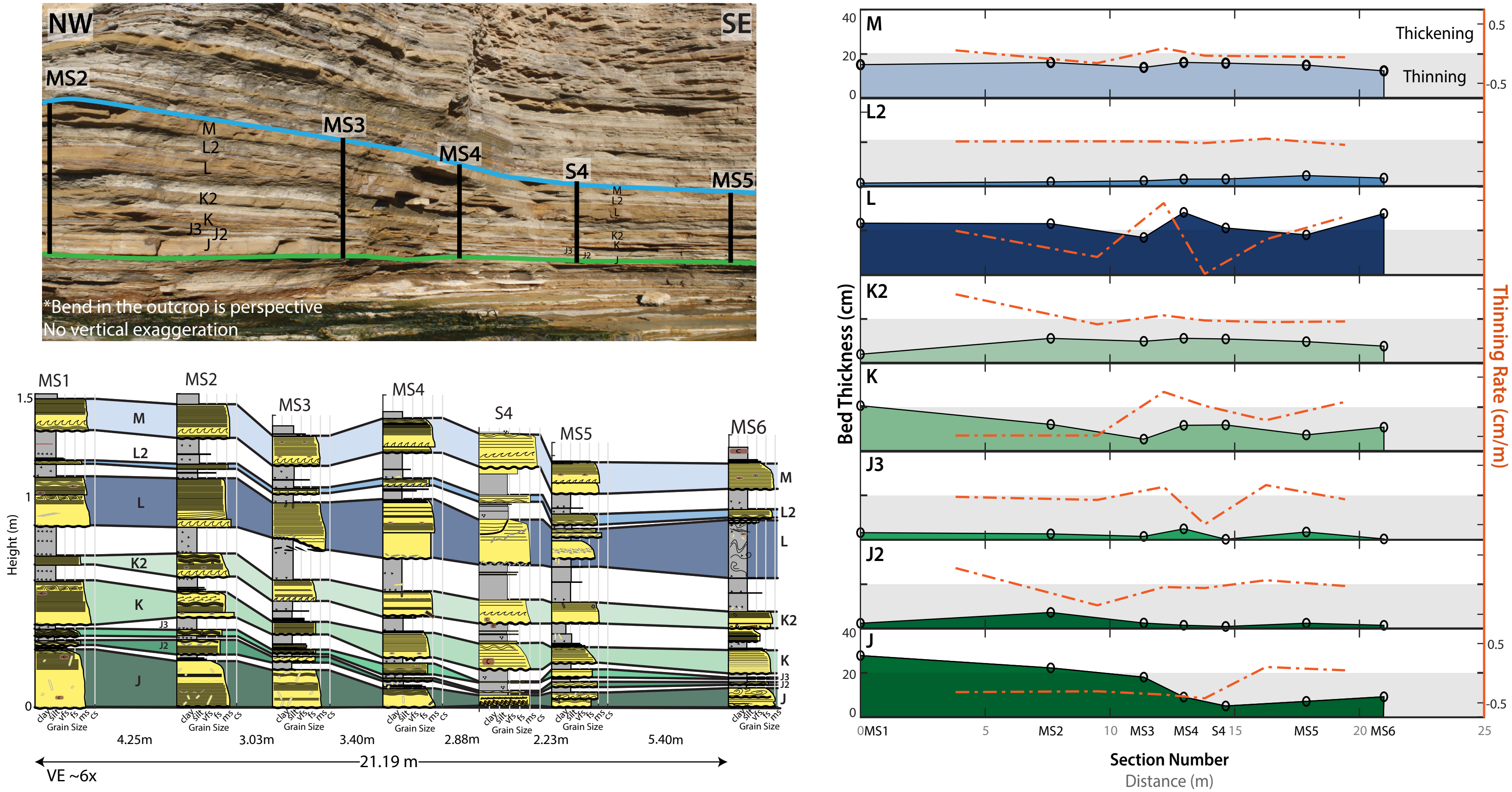

Figure 13: Outcrop photo (top left) and correlation panel (bottom left) with colors indicated associated element from figure 3. Bed compensation occurs within Element Three, predominantly in beds thicker than 10 cm. Plot contains bed thickness (m) on the left Y axis (black), thinning rate (cm/m) on the right Y axis (red), with the X axis showing lateral distance (m). Section locations marked with open circles.

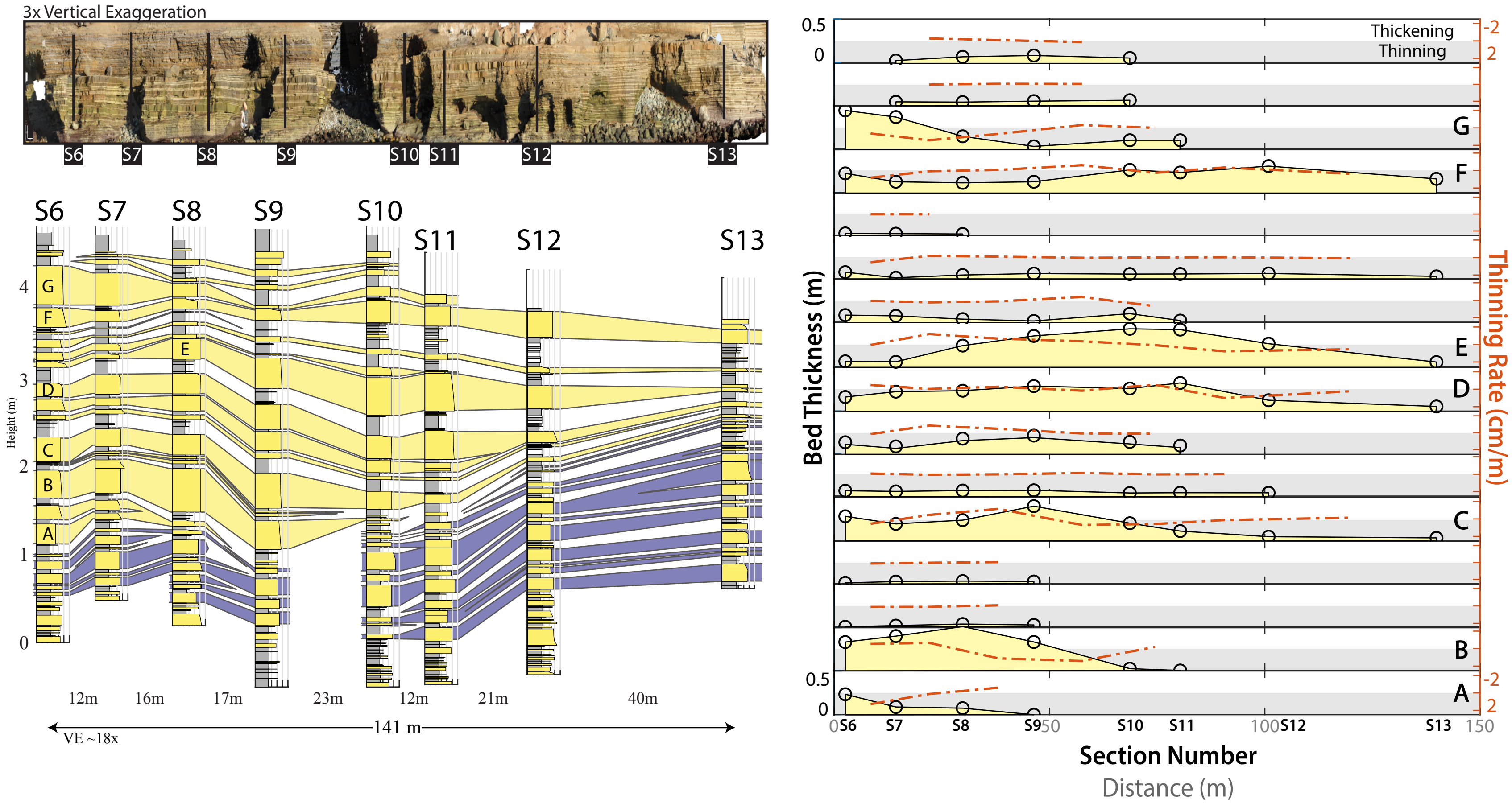

Figure 14: Inter-element compensation (Element 1 to Element 2) with internal intra-element compensation in Element 2. Plot contains bed thickness (m) on the left axis, thinning rate (cm/m) on the right axis in red, distance (m) on the bottom axis with section locations marked with open circles.

event bed. This manifests in outcrop through subtle pinching and swelling of each bed (Figure 13). However, beds thinner than 10 cm rarely display bed compensation, which could suggest the size of the flow has control on the extent of the bed scale compensation (Figure 13 & Figure 14). The increase in the degree of compensation from beds to elements indicates a hierarchical rather than fractal stacking method in these submarine lobe deposits (Straub and Pyles, 2012; Figure 14). For example, event beds within Element Two (yellow) infill the topography created by lobe Element One (purple) as well as the previous bed deposited within Element Two (Figure 14). Once Element Two has completely minimized the relief created by Element One (purple), it is able to redistribute the bed thickness more evenly across the depositional surface causing a decrease in thinning rate, as seen in bed E (Figure 14).

Using the understanding that compensation decreases from proximal-to-distal (Sullivan et al.,2000; Fernandez et al., 2014), the fairly abrupt outcrop expression of the contact between Element One and Two over approximately 50 m indicates a more proximal or axial lobe position than previously interpreted by Fleming (2010). This is supported by the relatively coarse-grained nature of the lobe deposits at Cabrillo National Monument (Figure 15). However, Elements Three and Four do not show large-magnitude compensation, suggesting that these are more distal or marginal lobe positions (Figure 11). Given that the event bed parameters are not discernible between Elements Two, Three, and Four (Figure 15), this may indicate a minor lateral switching of lobe elements rather than a larger-scale progradational/retrogradational pattern.

For distal submarine lobe deposits, the prevailing understanding is that sandstone bed thickness changes minimally over hundreds of meters (Walker & Mutti, 1973; Ricci-Lucchi, 1975; Shanmugam & Moiola, 1988). However, distal lobe deposits can also show abrupt thickness variations along-strike indicating a finger-like “dendritic” pattern (Twichell et al., 1992; Prélat et al., 2009; Talling et al., 2010) rather than a simple radial sheet commonly found in schematic models (Mutti and Normark, 1987). The low thinning rate values from distal locales (Figure 7) suggests that neither the Point Loma nor the compiled distal lobe deposits contain these dendritic features, or that they are not sampled or recognized within the extent of the outcrops and within the database. This could be due to the dendritic patterns only having slight thickness variations or that the sampling distance between measured sections is too large to truly document these dendritic features. For example, the 'pinch and swell' geometry found in the Point Loma Formation could be evidence of dendritic planform patterns (Figure 13), but the detailed analysis is beyond the scope of this study.

Inter-Lobe Element Architecture: Results

Whereas Element One does not show the true element thickness, lateral net-to-gross remains fairly consistent (Figure 11). Element Two shows an increase in net-to-gross from S1 to S8 (0.5 to 0.75) where the bed-scale compensation is occurring, then a decreases from S8 to S13 (0.75 to 0.45) where event beds thin and onlap onto Element One. Element Three shows two separate patterns of north to south decrease in net-to-gross between S1 to S4 and S6 to S10 (Figure 11). Whereas Element Four does not represent the true element thickness due to top truncation by modern erosion, the lateral net-to-gross within Element Four remains quite consistent (Figure 11). Because of the observable stratal architecture that defines these elements (Figure 11), expected to see separation between cross-plots of event bed parameters (Figure 15). For example, Element Two (light yellow) displays moderate fining rates, high thinning rates, high bed thicknesses, and moderate to high grain sizes, whereas Element Three (light green) displays the lowest fining rates, moderate thinning rates, high bed thicknesses, and the coarsest grain size. Element One (purple) and Element Four (blue) have the highest degree similarity for all parameters mentioned based on median location and KDE contour shapes (Figure 15). However, there is no clear separation to quantitatively identify the individual lobe elements using grain size, fining rates, bed thickness, and thinning rates based on their KDE contours at this outcrop location (Figure 15).

As the data are non-normal with small sample sizes, we statistically tested their similarity using a Kruskal-Wallis test (Kruskal and Wallis, 1952). Using a standard alpha of 0.05, the results showed we am unable to reject the null hypothesis that grain size, fining rate, and thinning rate by element have the same mean rank (p-values ranging from 0.0668 to 0.9920). However, Element Two has a statistically different mean rank of bed thickness compared to Elements One and Three with p-values of 0.0173 and 0.0033, respectively.

Inter-Lobe Element Architecture: Analysis

Even though there are well-defined stratal architectures that separate the lobe elements (Figure 10, 3), the event bed parameters (bed thickness, thinning rate, grain size, fining rate) are all very similar to each other for Elements One, Three and Four (Figure 15). These similarities suggest that the elements are quite similar to one another in terms of their architectural position (e.g., medial, off-axis) and sediment supply characteristics. If there are minimal changes in architectural positions between lobe elements, this would indicate a more hierarchical method of compensational stacking as the degree of bed compensation is small compared to the degree of element compensation (Mutti and Sonnino, 1981; Mutti and Normark, 1987; Deptuck et al., 2008; Prélat et al., 2009; Straub and Pyles, 2012). However, Element Two displays statistically different bed thicknesses compared to Elements One and Three, which could indicate a slight shift in architectural position, as all other parameters are statistically similar (Figure 15).

One potential downfall of this comparison is that each lobe element contains thin beds regardless of the overall thickness pattern. For example, as each event bed in a 'thick-bedded' element (e.g., Element Two) is traced laterally toward its pinch-out point, it approaches similar thicknesses as other, dominantly 'thin bedded' elements (e.g., Element One), creating overlap in parameter distributions (Figure 15). Also, the outcrop exposures at Cabrillo are small (width of ~300 m x thickness of ~8 m) relative to the dimensions of modern lobe elements (confined lobe element (range) - length x width x thickness: 300 - 5,000 m x 300 - 2,000 m x 10 – 20 m; unconfined lobe element (range) – length x width x thickness: 400 - 300,000 m x 1,000 -10,000 m x 1 – 2 m from Pettinga et al., in review), limiting the lateral and vertical event bed characteristics shown in Figure 15. With the restricted exposure near or less than the lowest width and thickness values of modern unconfined and confined lobe elements, this data probably represents less than a half of the lateral extent of a single lobe element.

Comparison to the Compilation Database

Using the compilation database, we are able to compare bed scale parameters of the Point Loma Formation at the Cabrillo National Monument to other submarine depositional environments (Figure 2, Figure 3, Figure 6, Figure 7 and Figure 8). The Point Loma Formation displays moderate thinning rates of .003 cm/m to 2 cm/m and bed thicknesses between 1 cm and 90 cm, which is lower than all other deposits, possibly due to the fine-scale correlation performed by this study (Figure 2, Figure 6, and Figure 11). Without these thinner beds (which many panels did not correlate, see Table 1), the Point Loma Fm. would plot similarly in thickness and thinning rate to the bulk of the lobe and channel-lobe transition zone populations. The Point Loma Fm. falls similar to the bulk population of lobes in thinning rate and lateral distance (Figure 3). To further refine the depositional environment of the Point Loma Formation at the Cabrillo National Monument, we utilize the interpreted lobe sub-environments from other outcrops to assess the similarities and differences in bed scale parameters (Figure 7). The Point Loma Formation at the Cabrillo National Monument is most comparable in bed thicknesses, thinning rates, and lateral bed continuity to semi-confined lobe deposits (Figure 7). The Point Loma Formation's net-to-gross median is most similar to confined or semi-confined distal settings. However, it's very tight net-to-gross distribution ranging between 0.5 and 0.75 perhaps reflects a sampling bias due to outcrop exposure and my relatively small scale of investigation.

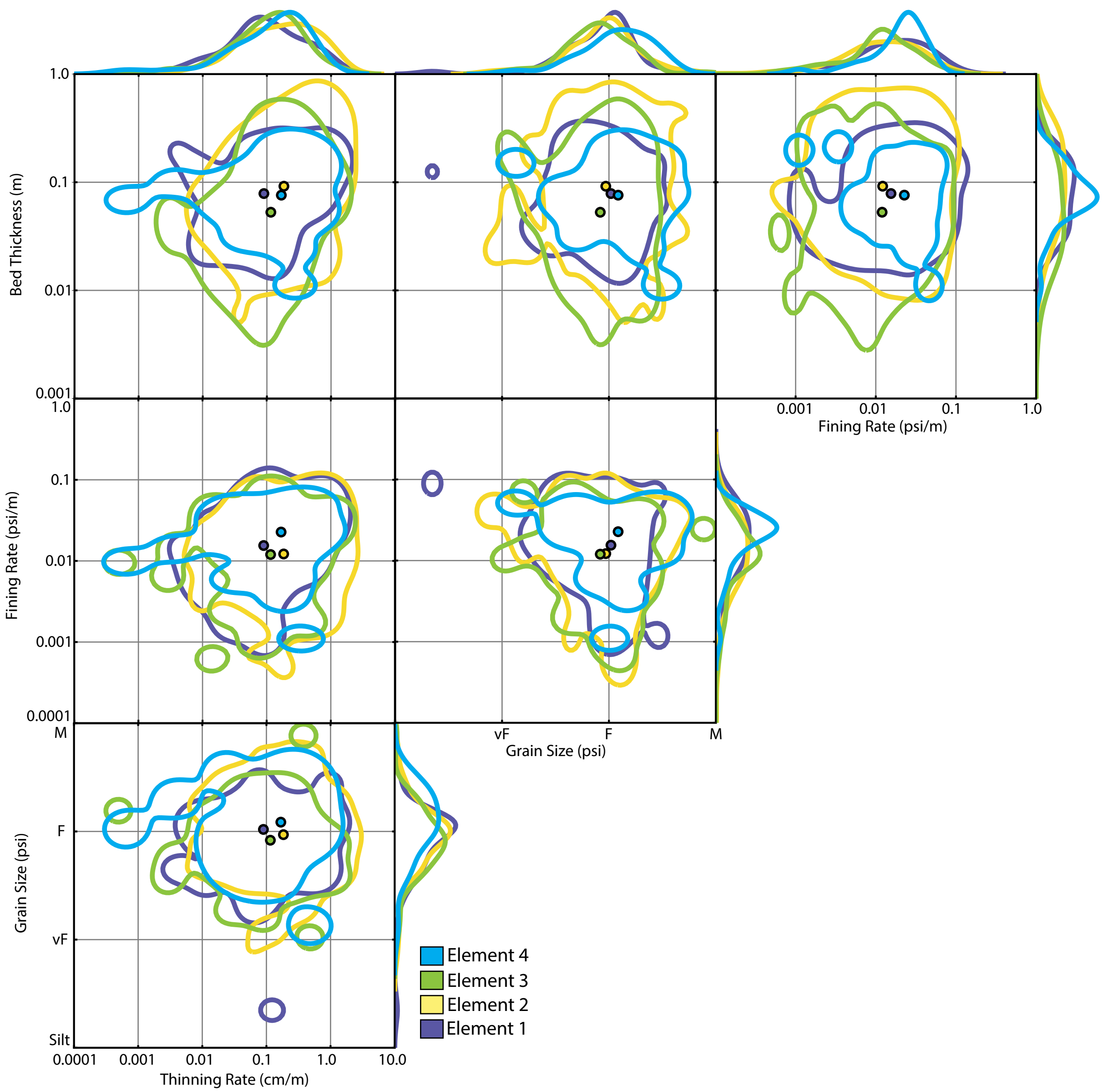

Figure 15: Element bed parameter plots displaying there is no clear separation within parameters to quantitatively determine lobe elements with grain size, fining rates, bed thickness, and thinning rates based on their KDE contours. Plots contain bed thickness (m), grain size (phi), magnitude of thinning rate (cm/m), and fining rate (phi/m) with a 60% KDE and median for each element.

Discussion

Refining the Point Loma Formation Environment

Through comparison to my newly created global database (Figure 2, Figure 3, Figure 6, Figure 7; Table 1) and detailed depositional models of submarine lobe deposition (e.g., Mutti and Normark, 1987; Deptuck et al., 2008; Prélat et al., 2009, 2010), we can refine the interpretation of the Point Loma Formation at Cabrillo National Monument. Based on the overall bed thicknesses, thinning rates, correlation distances and outcrop architectures the Point Loma Formation is most similar to lobes (Figure 6). The intermediate and approximately equal values of sandstone and mudstone bed thicknesses, abundant preservation of mudstone displayed in the moderate net-to-gross value (~ 0.5), the higher sandstone thinning rates that mudstone thinning rates, and the overall moderate lithology thinning rate suggests that the Point Loma is semi-confined rather than unconfined (cf. Fleming, 2010). This result is likely given deposition occurred within a forearc basin during active subduction (Nilsen and Abbott, 1981). Secondly, the abrupt element compensation, lack of erosion but high degree of mud clasts, high organic matter, and lower fine to upper medium grain sizes suggest that the Point Loma deposits at Cabrillo National Monument are more medial than previously interpreted (cf. Fleming, 2010; Stammer 2014).

How to Appropriately Apply Quantified Data

These quantified bed-scale parameter comparisons enable the recognition of (1) architectural similarities and differences between environments and (2) sub-environments within lobe deposits (e.g., medial vs. distal, confined vs. unconfined). This study also provides quantitative and statistical insights into lateral variability within and among submarine depositional deposits and provides quantitative data for constructing realistic geologic and reservoir models, particularly in data-poor settings where lateral lithology variability at the bed-scale is not observable and a major uncertainty (Hofstra et al., 2017) (Figure 6). For example, the bed thickness and thinning rate distributions (Figure 2) can help refine the interpretation of core data and constrain well log correlations, providing more confident classification of depositional environment. However, this newly created database relies on the assumption that the interpretation of depositional environment (Table 1) is correct. This assumption is intensified in lobe subenvironments, where differences may be minimal and subjectively defined (cf. Prélat and Hodgson, 2013). Therefore, caution is urged when using data from this study, as they were created using interpretations derived from natural outcrop exposures that often are ambiguous. These issues underscore the need for more quantification of these metrics to create a robust dataset and to avoid solely using qualitative based outcrop interpretations.

Summary and Conclusions

To understand and quantify lateral heterogeneity of turbidite event-beds across different submarine depositional environments, we compiled previously published bed-scale correlation panels from channel, levee, channel-lobe-transition-zone, lobe, and basin-plain deposits. Almost 30,000 individual measurements of event bed parameters indicate that neither bed thickness nor net-to-gross alone are useful for distinguishing depositional environment. For example, bed thickness ranges overlap across all environments and net-to-gross values display are very similar for (1) channel deposits, channel-lobe-transition-zone deposits, and lobe deposits and (2) levee deposits and basin-plain deposits. However, utilizing a combination of thinning rate, bed thickness, and correlation distance (i.e., the distance over which thinning rate is measured), clear boundaries can be established between deposits from different submarine depositional environments. For example, lobe deposits show thinner sandstone and mudstone beds compared to basin-plain deposits, but lobe deposits have much higher thinning rates over lower correlation distances. However, lobe deposits exhibit the most variability in thinning rate and bed thickness (likely due to the (1) extreme facies variability in lobe deposits and (2) differing sediment supply, basin configuration, and tectonic setting of the compiled database), and consequently lobe deposits would be very difficult to confidently distinguish from other environments in the subsurface**.** we sub-classified lobe deposits to provide a more detailed analysis into unconfined, semiconfined and confined settings. The data confirm that confined lobes have thicker sandstone and mudstone beds and lower net-to-gross values as compared to unconfined and semiconfined lobes. However, the results for semiconfined lobes indicate that the degree of lobe confinement and subenvironment is not easily interpretable at the outcrop scale. This uncertainty could be partially caused by subjectivity of qualitative interpretations of environment, which demonstrates the need for more quantitative studies of bed-scale heterogeneity. Sandstone and mudstone lithologies display different bed thickness and thinning rate relationships within each deposit, providing another method for environment identification and also provide valuable insights for downslope flow evolution and the construction of stratigraphic architecture. For example, channels commonly show thicker sandstone beds that thin more rapidly than mudstone beds. The results from this study are immediately applicable to parameterizing forward stratigraphic models as well as constraining property distribution in reservoir models of submarine lobe deposits as well as other submarine depositional environments.

To apply the results from the compilation study, we also studied submarine lobe strata of the Upper Cretaceous Point Loma Formation at Cabrillo National Monument near San Diego, California. These outcrops have previously been interpreted as distal submarine lobe deposits; however, the grain size, thinning rates and lateral bed variability are larger than predicted by classic models of distal lobe deposition. The difference in the degrees of bed-scale and lobe-element scale compensation in these deposits indicates a hierarchical (rather than fractal) method of compensation. The degree of compensation between lobe elements influences the resultant element net-to-gross at that location, which affects the ability to determine element boundaries in outcrop and within the subsurface (e.g., a core). Although clearly defined stratal surface separate lobe elements, architectural parameters of event beds (e.g., bed thickness, lateral correlation distance, thinning rate, fining rate) are not appreciably different between lobe elements, perhaps suggesting a similarity in architectural position across lobe elements. The Point Loma Formation deposits at the Cabrillo National

Monument have bed thicknesses and thinning rates most similar to semi-confined proximal lobes, suggesting a more proximal position than previously interpreted. Based on the grain size, relationships between sandstone and mudstone thicknesses and thinning rates, bed and lobe-element compensation, and minimal observed erosion, we reinterpret the Cabrillo National Monument section of the Point Loma Formation as a medial lobe with some degree of lateral and/or frontal confinement.

Acknowledgments

We acknowledge, Piret Plink-Bjorklund, Jeffrey May, and Fabien Laugier, for providing extremely insightful comments throughout this project. We thank Alexandra Fleming and Jane Stammer for leading the preliminary field trip and providing an excellent introduction to the Point Loma Formation. Lauren Bane, Mimi Do, Clark Gilbert, Pengfei Hou, Luke Pettinga, Lauren Shumaker, and James Smith IV for enduring field work on the California coast. We are also very appreciative of Keith Lombardo at the Cabrillo National Monument for allowing us access to the sea cliffs and providing equipment needed for all field seasons. We also thank Morgan Sullivan and Jeremiah Moody for their help in the field and for pitching so many great questions and ideas. RF acknowledges the funding support from the Chevron Center for Research Excellence (CoRE) at Colorado School of Mines, AAPG Grants-in-Aid, and GSA.

References

Al-Siyabi, H.A., 2000. Anatomy of a type II turbidite depositional system: Upper Jackfork Group, Degray Lake area, Arkansas. Special Publication-SEPM, 68, pp.245-262.

Amy, L.A. and Talling, P.J., 2006. Anatomy of turbidites and linked debrites based on long distance (120× 30 km) bed correlation, Marnoso Arenacea Formation, Northern Apennines, Italy. Sedimentology, 53(1), pp.161-212.

Atwater, T., 1970. Implications of plate tectonics for the Cenozoic tectonic evolution of western North America. Geological Society of America Bulletin, 81(12), pp.3513-3536.

Bersezio, R., Felletti, F. Riva, S. and Micucci, L., 2009. Trends in bed thickness and facies of turbiditic sandstone bodies: unravelling the effects of basin confinement, depositional processes, and modes of sediment supply. External controls on deep-water depositional systems, 92, pp.303-324.

Bigi, S., Milli, S., Corrado, S., Casero, P., Aldega, L., Botti, F., Moscatelli, M., Stanzione, O., Falcini, F., Marini, M. and Cannata, D., 2009. Stratigraphy, structural setting and burial history of the Messinian Laga basin in the context of Apennine foreland basin system. Journal of Mediterranean Earth Sciences, 1, pp.61-84.

Bouma, A. H., 1962. Sedimentology of some flysch deposits. A graphic approach to facies interpretation. Book - Amsterdam: Elsevier Pub. Co., pp.1-168.

Brunt, R.L., Hodgson, D.M., Flint, S.S., Pringle, J.K., Di Celma, C., Prélat, A. and Grecula, M., 2013. Confined to unconfined: anatomy of a base of slope succession, Karoo Basin, South Africa. Marine and Petroleum Geology, 41, pp.206-221.

Brunt, R.L., McAffrey, W.D. and Kneller, B.C., 2004. Experimental modeling of the spatial distribution of grain size developed in a fill-and-spill mini-basin setting. Journal of Sedimentary Research, 74(3), pp.438-446.

Cantelli, A., Pirmez, C., Johnson, S. and Parker, G., 2011. Morphodynamic and stratigraphic evolution of self-channelized subaqueous fans emplaced by turbidity currents. Journal of Sedimentary Research, 81(3), pp.233-247.

Carvajal, C., Paull, C.K., Caress, D.W., Fildani, A., Lundsten, E., Anderson, K., Maier, K.L., McGann, M., Gwiazda, R. and Herguera, J.C., 2017. Unraveling the Channel–Lobe Transition Zone With High-Resolution AUV Bathymetry: Navy Fan, Offshore Baja California, Mexico. Journal of Sedimentary Research, 87(10), pp.1049-1059.

Chapin, M., Tiller, G., Nilsen, T.H., Shew, R.D., Steffens, G.S. and Studlick, J.R.J., 2007. Synthetic seismic modeling of turbidite outcrops. Atlas of deep-water outcrops: AAPG Studies in Geology, 56, pp.21-25.

Chapin, M., 2007, Sheets and incised channels of the Kilcloher Cliff Section, Ross Formation Ireland, in Nilsen, T.H., Shew, R.D., Steffens, G.S. and Studlick, J.R.J., 2007. Atlas of deep-water outcrops: AAPG Studies in Geology 56. pp. 196-201.

Chapin, M., 2007B, Amalgamated sheet and channel sandstones at Kilbaha Bay, Ross Formation, Ireland, in Nilsen, T.H., Shew, R.D., Steffens, G.S. and Studlick, J.R.J., 2007. Atlas of deep-water outcrops: AAPG Studies in Geology 56. pp. 201-206.

Clare, M.A., Talling, P.J., Challenor, P., Malgesini, G. and Hunt, J., 2014. Distal turbidites reveal a common distribution for large (> 0.1 km^3) submarine landslide recurrence. Geology, 42(3), pp.263-266.

Clark, J.D., 1998. Scales of heterogeneity within the Ross Formation Turbidite System, County Clare, West Ireland. Department of Petroleum Engineering, Heriot-Watt University Confidential Report, pp.1-82.

Conway, K.W., Barrie, J.V., Picard, K. and Bornhold, B.D., 2012. Submarine channel evolution: active channels in fjords, British Columbia, Canada. Geo-Marine Letters, 32(4), pp.301-312.

Covault, J.A., Kostic, S., Paull, C.K., Sylvester, Z. and Fildani, A., 2017. Cyclic steps and related supercritical bedforms: building blocks of deep-water depositional systems, western North America. Marine Geology, 393, pp.4-20.

Croguennec, C., Ruffine, L., Dennielou, B., Baudin, F., Caprais, J.C., Guyader, V., Bayon, G., Brandily, C., Le Bruchec, J., Bollinger, C. and Germain, Y., 2017. Evidence and age estimation of mass wasting at the distal lobe of the Congo deep-sea fan. Deep Sea Research Part II: Topical Studies in Oceanography, 142, pp.50-63.

Damuth, J.E. and Flood, R.D., 1983. Morphology, sedimentation processes, and growth pattern of the Amazon deep-sea fan. Geo-Marine Letters, 3(2-4), pp.109-117.

Dennielou, B., Huchon, A., Beaudouin, C. and Berné, S., 2006. Vertical grain-size variability within a turbidite levee: Autocyclicity or allocyclicity? A case study from the Rhône neofan, Gulf of Lions, Western Mediterranean. Marine Geology, 234(1-4), pp.191-213.

Deptuck, M.E., Piper, D.J., Savoye, B. and Gervais, A., 2008. Dimensions and architecture of late Pleistocene submarine lobes off the northern margin of East Corsica. Sedimentology, 55(4), pp.869-898.

Drinkwater, N.J., 1995. Sheet-like turbidite system: the Kongsfjord Formation, Finnmark, north Norway. In Atlas of Deep Water Environments, Springer, Dordrecht, pp.267-274.

Drinkwater, N.J. and Pickering, K.T., 2001. Architectural elements in a high-continuity sand-prone turbidite system, late Precambrian Kongsfjord Formation, northern Norway:

Application to hydrocarbon reservoir characterization. AAPG bulletin, 85(10), pp.1731-1757.

Elliott, T., 2000. Megaflute erosion surfaces and the initiation of turbidite channels. Geology, 28(2), pp.119-122.

Etienne, S., Mulder, T., Bez, M., Desaubliaux, G., Kwasniewski, A., Parize, O., Dujoncquoy, E. and Salles, T., 2012. Multiple scale characterization of sand-rich distal lobe deposit variability: examples from the Annot Sandstones Formation, Eocene–Oligocene, SE France. Sedimentary Geology, 273, pp.1-18.

Felletti, F., 2002. Complex bedding geometries and facies associations of the turbiditic fill of a confined basin in a transpressive setting (Castagnola Fm., Tertiary Piedmont Basin, NW Italy). Sedimentology, 49(4), pp.645-667.

Fernandez, R.L., Cantelli, A., Pirmez, C., Sequeiros, O. and Parker, G., 2014. Growth Patterns of Subaqueous Depositional Channel Lobe Systems Developed Over A Basement With A Downdip Break In Slope: Laboratory ExperimentsGrowth Patterns Of Depositional Channel Lobe Systems. Journal of Sedimentary Research, 84(3), pp.168-182.

Fildani, A., Normark, W.R., Kostic, S. and Parker, G., 2006. Channel formation by flow stripping: Large-scale scour features along the Monterey East Channel and their relation to sediment waves. Sedimentology, 53(6), pp.1265-1287.

Fleming, A., 2010. Stratigraphic architecture of lobe strata in a submarine fan setting, Point Loma Formation, California (Master's Thesis, Colorado School of Mines. Arthur Lakes Library), pp.1-143.

Fonnesu, M., Patacci, M., Haughton, P.D., Felletti, F. and McCaffrey, W.D., 2016. Hybrid event beds generated by local substrate delamination on a confined-basin floor. Journal of Sedimentary Research, 86(8), pp.929-943.

Fonnesu, M., Felletti, F., Haughton, P.D., Patacci, M. and McCaffrey, W.D., 2018. Hybrid event bed character and distribution linked to turbidite system sub-environments: The North Apennine Gottero Sandstone (north-west Italy). Sedimentology, 65(1), pp.151-190.

Ghosh, B. and Lowe, D.R., 1993. The architecture of deep-water channel complexes, Cretaceous Venado sandstone member, Sacramento Valley, California. Advances in the Sedimentary Geology of the Great Valley Group, Sacramento Valley California. Pacific Section – SEPM, 73, pp.51-65.

Girty, G.H., 1987. Sandstone provenance, Point Loma Formation, San Diego, California: evidence for uplift of the Peninsular Ranges during the Laramide orogeny. Journal of Sedimentary Research, 57(5), pp.839–844.

Groenenberg, R.M., Hodgson, D.M., Prelat, A., Luthi, S.M. and Flint, S.S., 2010. Flow–deposit interaction in submarine lobes: Insights from outcrop observations and realizations of a process-based numerical model. Journal of Sedimentary Research, 80(3), pp.252-267.

Haughton, P., 2001. Contained turbidites used to track sea bed deformation and basin migration, Sorbas Basin, south-east Spain. Basin Research, 13(2), pp.117-139.

Haughton, P., Davis, C., McCaffrey, W. and Barker, S., 2009. Hybrid sediment gravity flow deposits–classification, origin and significance. Marine and Petroleum Geology, 26(10), pp.1900-1918.

Hazeu, G.J., Krakstad, O.S., Rian, D.T. and Skaug, M., 1988. The application of new approaches for shale management in a three-dimensional simulation study of the Frigg Field. SPE Formation Evaluation, 3(03), pp.493-502.

Hilton, V.C. and Pickering, K.T., 1995. The Montagne de Chalufy turbidite onlap, Eocene-Oligocene turbidite sheet system, Hautes Provence, SE France. In Atlas of Deep Water Environments, pp. 236-241. Springer, Dordrecht.

Hiscott, R.N., 1980. Depositional framework of sandy mid-fan complexes of Tourelle Formation, Ordovician, Quebec. AAPG Bulletin, 64(7), pp.1052-1077.

Hiscott, R.N. and Middleton, G.V., 1979. Depositional mechanics of thick-bedded sandstones at the base of a submarine slope, Tourelle Formation (Lower Ordovician), Quebec, Canada. SEPM Special Publication, 27, pp.307-326.

Hiscott, R.N., Pickering, K.T. and Beeden, D.R., 1986. Progressive filling of a confined Middle Ordovician foreland basin associated with the Taconic Orogeny, Quebec, Canada. Foreland basins, pp.307-325.

Hiscott, R.N., Hall, F.R. and Pirmez, C., 1997. Turbidity-current overspill from the Amazon Channel: texture of the silt/sand load, paleoflow from anisotropy of magnetic susceptibility, and implications for flow processes. In Proceedings-Ocean Drilling Program Scientific Results. pp. 53-78.

Hofstra, M., Hodgson, D.M., Peakall, J. and Flint, S.S., 2015. Giant scour-fills in ancient channel-lobe transition zones: Formative processes and depositional architecture. Sedimentary Geology, 329, pp.98-114.

Hofstra, M., Pontén, A.S.M., Peakall, J., Flint, S.S., Nair, K.N. and Hodgson, D.M., 2017. The impact of fine-scale reservoir geometries on streamline flow patterns in submarine lobe deposits using outcrop analogues from the Karoo Basin. Petroleum Geoscience, 23(2), pp.159-176.

Hubbard, S.M., Covault, J.A., Fildani, A. and Romans, B.W., 2014. Sediment transfer and deposition in slope channels: deciphering the record of enigmatic deep-sea processes from outcrop. GSA Bulletin, 126(5-6), pp.857-871.

Hubbard, S.M., Romans, B.W. and Graham, S.A., 2008. Deep-water foreland basin deposits of the Cerro Toro Formation, Magallanes basin, Chile: Architectural elements of a sinuous basin axial channel belt. Sedimentology, 55(5), pp.1333-1359.

Ito, M., 1997. Spatial variation in turbidite-to-contourite continuums of the Kiwada and Otadai formations in the Boso Peninsula, Japan: An unstable bottom-current system in a Plio-Pleistocene forearc basin. Journal of Sedimentary Research, 67(3), pp.571-582.

Jegou, I., Savoye, B., Pirmez, C. and Droz, L., 2008. Channel-mouth lobe complex of the recent Amazon Fan: The missing piece. Marine Geology, 252(1-2), pp.62-77.

Jobe, Z.R., Bernhardt, A. and Lowe, D.R., 2010. Facies and architectural asymmetry in a conglomerate-rich submarine channel fill, Cerro Toro Formation, Sierra del Toro, Magallanes Basin, Chile. Journal of Sedimentary Research, 80(12), pp.1085-1108.

Jobe, Z.R., Sylvester, Z., Howes, N., Pirmez, C., Parker, A., Cantelli, A., Smith, R., Wolinsky, M.A., O'Byrne, C., Slowey, N. and Prather, B., 2017. High-resolution, millennial-scale patterns of bed compensation on a sand-rich intraslope submarine fan, western Niger Delta slope. GSA Bulletin, 129(1-2), pp.23-37.

Jobe, Z.R., Howes, N., Romans, B.W. and Covault, J.A., 2018. Volume and recurrence of submarine-fan-building turbidity currents. The Depositional Record, 0(0), pp. 1-17

Joseph, P., Callec, Y. and Ford, M., 2012. Dynamic Controls on Sedimentology and Reservoir Architecture in the Alpine Foreland Basin: A Field Guide to the Eocene–Oligocene Grès d'Annot Turbidite System of SE France. France, IFP Energies Nouvelles e-books.

Joseph, P. and Lomas, S.A., 2004. Deep-water sedimentation in the Alpine foreland basin of SE France: New perspectives on the Grès d'Annot and related systems—An introduction. Geological Society, London, Special Publications, 221(1), pp.1-16.

Kane, I.A. and Pontén, A.S., 2012. Submarine transitional flow deposits in the Paleogene Gulf of Mexico. Geology, 40(12), pp.1119-1122.

Kern, J.P. and Warme, J.E., 1974. Trace fossils and bathymetry of the Upper Cretaceous Point Loma Formation, San Diego, California. Geological Society of America Bulletin, 85(6), pp.893-900.

Kennedy, M.P., 1975. Geology of the San Diego metropolitan area, California: California Division of Mines and Geology, Bulletin 200, Section A, pp. 9-39, plates.

Kennedy, M.P. and Moore, G.W., 1971. Stratigraphic relations of upper Cretaceous and Eocene formations, San Diego coastal area, California. AAPG Bulletin, 55(5), pp.709-722.

Kennedy, M.P., Tan, S.S., Bovard, K.R., Garcia, A.G. and Burns, D., 2008. Geologic Map of the San Diego 30′ X 60′ Quadrangle, California. California Geological Survey, pp.1-21.

Kerans, C., Lucia, F.J. and Senger, R.K., 1994. Integrated characterization of carbonate ramp reservoirs using Permian San Andres Formation outcrop analogs. AAPG bulletin, 78(2), pp.181-216.

Keevil, G.M., Peakall, J., Best, J.L. and Amos, K.J., 2006. Flow structure in sinuous submarine channels: velocity and turbulence structure of an experimental submarine channel. Marine Geology, 229(3-4), pp.241-257.

Konsoer, K., Zinger, J. and Parker, G., 2013. Bankfull hydraulic geometry of submarine channels created by turbidity currents: relations between bankfull channel characteristics and formative flow discharge. Journal of Geophysical Research: Earth Surface, 118(1), pp.216-228.

Kruskal, W.H. and Wallis, W.A., 1952. Use of ranks in one-criterion variance analysis. Journal of the American Statistical Association, 47(260), pp.583-621.

Lamb, M.P., Toniolo, H. and Parker, G., 2006. Trapping of sustained turbidity currents by intraslope minibasins. Sedimentology, 53(1), pp.147-160.

Lien, T., Walker, R.G. and Martinsen, O.J., 2003. Turbidites in the Upper Carboniferous Ross Formation, western Ireland: reconstruction of a channel and spillover system. Sedimentology, 50(1), pp.113-148.

Lowe, D.R., 1982. Sediment gravity flows: II Depositional models with special reference to the deposits of high-density turbidity currents. Journal of Sedimentary Research, 52(1), pp. 279–297.

Macauley, R.V. and Hubbard, S.M., 2013. Slope channel sedimentary processes and stratigraphic stacking, Cretaceous Tres Pasos Formation slope system, Chilean Patagonia. Marine and Petroleum Geology, 41, pp.146-162.

Marini, M., Felletti, F., Milli, S. and Patacci, M., 2016. The thick-bedded tail of turbidite thickness distribution as a proxy for flow confinement: Examples from tertiary basins of central and northern Apennines (Italy). Sedimentary Geology, 341, pp.96-118.

Marini, M., Milli, S., Ravnås, R. and Moscatelli, M., 2015. A comparative study of confined vs. semi-confined turbidite lobes from the Lower Messinian Laga Basin (Central Apennines, Italy): implications for assessment of reservoir architecture. Marine and Petroleum Geology, 63, pp.142-165.

Marshall, M. and McNaboe, J., 1984. Preliminary paleomagnetic results from the Cretaceous Point Loma Formation. Upper Cretaceous Depositional Systems, Southern California, SEPM Pacific Section, pp. 1.

May, J. A., Lohmar, J. M., Warme, J. E., & Morgan, S. (1991). Early to middle Eocene La Jolla Group of Black's Beach. La Jolla, California: SEPM, Pacific Section, Fieldtrip Guidebook, 68, pp. 27-36.

May, J. A., & Warme, J. E. (1991). Marine Sedimentology of the early to middle Eocene La Jolla Group. In Abbott, P. L. and May, J. A., eds. 1991 Eocene Geologic History, San Diego Region, Pacific section SEPM, 68, pp. 73-88.

May, J.A. and Warme, J.E., 2007. An ancient submarine canyon, Black's Beach, La Jolla, California, USA. Atlas of Deepwater Outcrops. American Association of Petroleum Geologists. SG56, CDROM.

Morris, W.R., Smith, D.P. and Busby-Spera, C.J., 1989. Deep marine conglomerate facies and processes in Cretaceous forearc basins of Baja California, Mexico. In Colburn, Ivan P., Patrick L. Abbott and John Minch, eds., 1989, Conglomerates in Basin Analysis: A Symposium Dedicated to A. O. Woodford: Pacific Section SEPM, 62, pp. 123-142.

Morris, W. and Busby-Spera, C., 1990. A submarine-fan valley-levee complex in the Upper Cretaceous Rosario Formation: Implication for turbidite facies models. Geological Society of America Bulletin, 102(7), pp.900-914.

Mutti, E. and Normark, W.R., 1987. Comparing examples of modern and ancient turbidite systems: problems and concepts. In Marine Clastic Sedimentology, pp.1-38. Springer, Dordrecht.

Mutti, E. and Sonnino, M., 1981. Compensation cycles: a diagnostic feature of turbidite sandstone lobes. In International Association of Sedimentologists, 2nd European Regional Meeting, Bologna, Abstracts, pp.120-123.

Nilsen, T.H. and Abbott, P.L., 1981. Paleogeography and sedimentology of upper Cretaceous turbidites, San Diego, California. AAPG Bulletin, 65(7), pp.1256-1284.

Nilsen, T.H. and Abbott, P.L., 1981. Paleogeography and sedimentology of upper Cretaceous turbidites, San Diego, California. AAPG Bulletin, 65(7), pp.1256-1284.

Nordstrom, C.E., 1970. Lusardi Formation: a post-batholithic Cretaceous conglomerate north of San Diego, California. Geological Society of America Bulletin, 81(2), pp.601-606.

Normark, W.R., 1978. Fan valleys, channels, and depositional lobes on modern submarine fans: characters for recognition of sandy turbidite environments. AAPG Bulletin, 62(6), pp.912-931.

Normark, W.R., 1989. Observed parameters for turbidity-current flow in channels, Reserve Fan, Lake Superior. Journal of Sedimentary Research, 59(3), pp.423-431.

Pantopoulos, G., Kneller, B.C., McArthur, A.D., Courivaud, S., Grings, A.E. and Kuchle, J., 2018. Turbidite bed thickness statistics of architectural elements in a deep-marine confined mini-basin setting: Examples from the Grès d'Annot Formation, SE France. Marine and Petroleum Geology, 95, pp.16-29.

Peakall, J., McCaffrey, B. and Kneller, B., 2000. A process model for the evolution, morphology, and architecture of sinuous submarine channels. Journal of Sedimentary Research, 70(3), pp.434-448.

Peterson, G.L., 1970. Distinctions between Cretaceous and Eocene conglomerates in the San Diego area, southwestern California. In Pacific Slope Geology of Northern Baja California and Adjacent Alta California: Guidebook, pp. 90-98.

Pettinga, L., Jobe, Z. R., Shumaker, L., & Howes, N. (in review). Morphometric scaling relationships in submarine channel-lobe systems: implications for turbidite depositional processes and stratigraphic architecture. Geology.

Pettingill, H. S., Braunsdorf, N. R., Cameron, C. S., Hottman, W. E., Keller, F. B., Neher, K. E., & Strauss, R. C., 1993, The Kongsfjord Formation outcrop study.

Pettingill, H.S. and Weimer, P., 2002. Worlwide deepwater exploration and production: Past, present, and future. The Leading Edge, 21(4), pp.371-376.

Picot, M., Droz, L., Marsset, T., Dennielou, B. and Bez, M., 2016. Controls on turbidite sedimentation: insights from a quantitative approach of submarine channel and lobe architecture (Late Quaternary Congo Fan). Marine and Petroleum Geology, 72, pp.423-446.

Piper, D.J. and Normark, W.R., 1983. Turbidite depositional patterns and flow characteristics, Navy submarine fan, California Borderland. Sedimentology, 30(5), pp.681-694.

Pirmez, C., Prather, B.E., Mallarino, G., O'Hayer, W.W., Droxler, A.W., Winker, C.D., Deptuck, M.E., Mohrig, D., Hoorn, B.V. and Wynn, R.B., 2012. Chronostratigraphy of the Brazos-Trinity depositional system, Western Gulf of Mexico: Implications for deep-water depositional models. Application of the principles of seismic geomorphology to continental-slope and base-of-slope systems: Case studies from seafloor and near-seafloor analogues: SEPM Special Publication, 99, pp.111-143.

Popenoe, W.P., 1973. Southern California Cretaceous formations and faunas with especial reference to the Simi Hills and Santa Monica Mountains. Cretaceous Stratigraphy of the Santa Monica Mountains and Simi Hills, Southern California. Pacific Section, SEPM, Geological Guidebook, Los Angeles, California, pp.15-20.

Prather, B.E., Booth, J.R., Steffens, G.S. and Craig, P.A., 1998. Classification, lithologic calibration, and stratigraphic succession of seismic facies of intraslope basins, deep-water Gulf of Mexico. AAPG Bulletin, 82(5), pp.701-728.

Prather, B.E., Pirmez, C.A.R.L.O.S., Winker, C.D., Deptuck, M.E. and Mohrig, D., 2012. Stratigraphy of linked intraslope basins: Brazos-Trinity system western Gulf of Mexico. Application of the principles of seismic geomorphology to continental-slope and base-of-slope systems: Case studies from seafloor and near-seafloor analogues: SEPM Special Publication, 99, pp.83-109.

Prélat, A., Covault, J.A., Hodgson, D.M., Fildani, A. and Flint, S.S., 2010. Intrinsic controls on the range of volumes, morphologies, and dimensions of submarine lobes. Sedimentary Geology, 232(1-2), pp.66-76.

Prélat, A. and Hodgson, D.M., 2013. The full range of turbidite bed thickness patterns in submarine lobes: controls and implications. Journal of the Geological Society, 170(1), pp.209-214.

Prélat, A., Hodgson, D.M. and Flint, S.S., 2009. Evolution, architecture and hierarchy of distributary deep-water deposits: a high-resolution outcrop investigation from the Permian Karoo Basin, South Africa. Sedimentology, 56(7), pp.2132-2154.

Pyles, D.R., 2008. Multiscale stratigraphic analysis of a structurally confined submarine fan: Carboniferous Ross Sandstone, Ireland. AAPG bulletin, 92(5), pp.557-587.

Pyles, D.R., Straub, K.M. and Stammer, J.G., 2013. Spatial variations in the composition of turbidites due to hydrodynamic fractionation. Geophysical Research Letters, 40(15), pp.3919-3923.

Pyrcz, M.J., Catuneanu, O. and Deutsch, C.V., 2005. Stochastic surface-based modeling of turbidite lobes. AAPG bulletin, 89(2), pp.177-191.

Remacha, E., Oms, O. and Coello, J., 1995. The Rapitán turbidite channel and its related eastern levee-overbank deposits, Eocene Hecho group, south-central Pyrenees, Spain. In Atlas of Deep Water Environments, pp. 145-149. Springer, Dordrecht.

Remacha, E. and Fernández, L.P., 2003. High-resolution correlation patterns in the turbidite systems of the Hecho Group (South-Central Pyrenees, Spain). Marine and Petroleum Geology, 20(6-8), pp.711-726.

Remacha, E., Fernández, L.P. and Maestro, E., 2005. The transition between sheet-like lobe and basin-plain turbidites in the Hecho Basin (South-Central Pyrenees, Spain). Journal of Sedimentary Research, 75(5), pp.798-819.

Ricci-Lucchi, F., 1975. Depositional cycles in two turbidite formations of northern Apennines. Journal of Sedimentary Research, 45(1), pp.3-43.

Romans, B.W., Normark, W.R., McGann, M.M., Covault, J.A. and Graham, S.A., 2009. Coarse-grained sediment delivery and distribution in the Holocene Santa Monica Basin, California: implications for evaluating source-to-sink flux at millennial time scales. Geological Society of America Bulletin, 121(9-10), pp.1394-1408.

Schuppers, J.D., 1993. Facies and architecture of deep-water Sandstone lobes: Comparison of a shale-rich and a sand-rich system. AAPG Bulletin, 77(9), Conference: American Association of Petroleum Geologists (AAPG) mid-continent section meeting, Amarillo, TX (United States), 10-12 Oct 1993.

Shanmugam, G. and Moiola, R.J., 1988. Submarine fans: characteristics, models, classification, and reservoir potential. Earth-Science Reviews, 24(6), pp.383-428.

Shew, R.D., 2007, Sheet, thin-bed, and channel architectures in the Tourelle Formation, Ste. Anne des Monts, Gaspe Peninsula, Canada, in Nilsen, T.H., Shew, R.D., Steffens, G.S. and Studlick, J.R.J., 2007. Atlas of deep-water outcrops: AAPG Studies in Geology 56. pp. 73-77.

Shumaker, L.E., Jobe, Z.R., Johnstone, S.A., Pettinga, L.A., Cai, D., and Moody, J.D., 2018 (in press), Controls on submarine channel-modifying processes identified through morphometric scaling relationships. Geosphere.

Silalahi, H.S.M.P., 2009. Stratigraphic architecture of slope deposits associated with prograding margins, Sobrarbe Formation: Ainsa Basin, Spain (Doctoral dissertation, Colorado School of Mines).

Slatt, R.M., Weimer, P. and Stone, C.G., 1997. Reinterpretation of depositional processes in a classic flysch sequence (Pennsylvanian Jackfork Group), Ouachita Mountains, Arkansas and Oklahoma: Discussion. AAPG bulletin, 81(3), pp.449-459.

Slatt, R.M., 2000. Why Outcrop Characterization of Turbidite Systems? AAPG Memoir 72/SEPM Special Publication, 68(17). pp. 181-185.

Sliter, W.V., 1979, Cretaceous foraminifers from La Jolla, California in Geological excursions in the Southern California area (Abbott, P.L. eds), Department of Geological Services: San Diego University, San Diego, pp. 171-172.

Sliter, W.V., 1984. Cretaceous foraminifers from La Jolla, California. Upper Cretaceous Depositional Systems, Southern California. Pacific Section – SEPM. pp. 35-36

Smith, D.P., Ruiz, G., Kvitek, R. and Iampietro, P.J., 2005. Semiannual patterns of erosion and deposition in upper Monterey Canyon from serial multibeam bathymetry. GSA Bulletin, 117(9-10), pp.1123-1133.

Smith, R.D.A., 1995. Complex bedding geometries in proximal deposits of the Castelnuovo Member, Rocchetta Formation, Tertiary Piedmont Basin, NW Italy. In Atlas of Deep Water Environments, pp. 244-24. Springer, Dordrecht.

Spychala, Y.T., Hodgson, D.M., Flint, S.S. and Mountney, N.P., 2015. Constraining the sedimentology and stratigraphy of submarine intraslope lobe deposits using exhumed examples from the Karoo Basin, South Africa. Sedimentary Geology, 322, pp.67-81.

Spychala, Y.T., Hodgson, D.M., Prélat, A., Kane, I.A., Flint, S.S. and Mountney, N.P., 2017. Frontal and lateral submarine lobe fringes: Comparing sedimentary facies, architecture and flow processes. Journal of Sedimentary Research, 87(1), pp.75-96.

Stammer, J.G., 2014. Hydrodynamic fractionation of minerals and textures in submarine fans: Quantitative analysis from outcrop, experimental, and subsurface studies. (Chapter 3: Doctoral Dissertation, Colorado School of Mines.)

Stephen, K.D., Clark, J.D. and Gardiner, A.R., 2001. Outcrop-based stochastic modelling of turbidite amalgamation and its effects on hydrocarbon recovery. Petroleum Geoscience, 7(2), pp.163-172.

Stevenson, C.J., Jackson, C.A.L., Hodgson, D.M., Hubbard, S.M. and Eggenhuisen, J.T., 2015. Deep-water sediment bypass. Journal of Sedimentary Research, 85(9), pp.1058-1081.

Stevenson, C.J., Talling, P.J., Sumner, E.J., Masson, D.G., Frenz, M. and Wynn, R.B., 2014. On how thin submarine flows transported large volumes of sand for hundreds of kilometres across a flat basin plain without eroding the sea floor. Sedimentology, 61(7), pp.1982-2019.

Straub, K.M. and Pyles, D.R., 2012. Quantifying the hierarchical organization of compensation in submarine fans using surface statistics. Journal of Sedimentary Research, 82(11), pp.889-898.

Stright, L., Stewart, J., Campion, K. and Graham, S., 2014. Geologic and seismic modeling of a coarse-grained deep-water channel reservoir analog (Black's Beach, La Jolla, California) Seismic Modeling of a Deep-Water Reservoir Outcrop Analog, California. AAPG bulletin, 98(4), pp.695-728.

Sullivan, M., Jensen, G., Goulding, F., Jennette, D., Foreman, L. and Stern, D., 2000, December. Architectural analysis of deep-water outcrops: Implications for exploration and development of the Diana sub-basin, western Gulf of Mexico. In Deep-water reservoirs of the world: Gulf Coast Section SEPM Foundation 20th Annual Research Conference, pp. 1010-1032.

Sumner, E.J., Talling, P.J., Amy, L.A., Wynn, R.B., Stevenson, C.J. and Frenz, M., 2012. Facies architecture of individual basin-plain turbidites: Comparison with existing models and implications for flow processes. Sedimentology, 59(6), pp.1850-1887.

Sylvester, Z., Cantelli, A. and Pirmez, C., 2015. Stratigraphic evolution of intraslope minibasins: Insights from surface-based model. AAPG Bulletin, 99(6), pp.1099-1129.

Talling, P.J., Wynn, R.B., Schmmidt, D.N., Rixon, R., Sumner, E. and Amy, L., 2010. How did thin submarine debris flows carry boulder-sized intraclasts for remarkable distances across low gradients to the far reaches of the Mississippi fan?. Journal of Sedimentary Research, 80(10), pp.829-851.

Tőkés, L. and Patacci, M., (in press). Quantifying tabularity of turbidite beds and its relationship to the inferred degree of basin confinement. Marine and Petroleum Geology.

Twichell, D.C., Schwab, W.C., Nelson, C.H., Kenyon, N.H. and Lee, H.J., 1992. Characteristics of a sandy depositional lobe on the outer Mississippi fan from SeaMARC IA sidescan sonar images. Geology, 20(8), pp.689-692.

Vipond, E., 2005, Modelling small-scale heterogeneities in a channelised turbidite system: Digital outcrop study from the Ainsa I Turbidite System. (Master's thesis: Bergen, Norway, University of Bergen).

Walker, R.G. and Mutti, E., 1973. Part IV. Turbidite facies and facies associations. Turbidites and Deep Water Sedimentation. Pacific Section – SEPM. pp. 119-157.

Weaver, P.P.E., Rothwell, R.G., Ebbing, J., Gunn, D. and Hunter, P.M., 1992. Correlation, frequency of emplacement and source directions of megaturbidites on the Madeira Abyssal Plain. Marine Geology, 109(1-2), pp.1-20.

Weber, K.J., 1982. Influence of common sedimentary structures on fluid flow in reservoir models. Journal of Petroleum Technology, 34(03), pp.665-672.

Weimer, P. and Pettingill, H.S., 2007. Deep-water exploration and production: A global overview. Atlas of deep-water outcrops: AAPG Studies in Geology, 56, p.12-16.

Wynn, R.B., Kenyon, N.H., Masson, D.G., Stow, D.A. and Weaver, P.P., 2002. Characterization and recognition of deep-water channel-lobe transition zones. AAPG bulletin, 86(8), pp.1441-1446.

Yeo, R.K., 1982. The stratigraphy and sedimentology of upper Cretaceous sediments of southwestern California and Baja California, Mexico (Doctoral dissertation, Rice University).

Zou, F., 2015. Integrated Study on Sequence Stratigraphic Framework of Deepwater Jackfork Group and Woodford Shale. (Doctoral Dissertation, The University of Oklahoma)

Supplemental Material A: Panel Projection Uncertainty

Commonly, researchers project correlation panels into strike or dip orientations to understand how the facies changes differ between those orientations. In this study, I am interested in lateral changes in bed thickness, but I only have quasi-2D outcrops (Figure 16). Applying a projection factor would correctly change the lateral correlation distance, but would incorrectly adjust bed thickness into the new architectural location (Figure 16) (Equation 1). Projecting the bed from the original section location along either A to A’ or B to B’ project lines changes the architectural location of the bed within the lobe (Figure 16A) and would need an imposed thinning rate along that projection line to account for a change in position within the lobe (Figure 16B). For example, as the bed is projected along A to A’, the bed location moves from an axial location to a more marginal location, but there is no available information to constrain how bed thickness would change because there is no outcrop in that location (Figure 16). Secondly, I do not have constraint on the lobe dimensions, so I cannot estimate the extent of architectural change. Therefore, applying a projection factor for this study is inappropriate because of the lack of data in the direction of the projected strike or dip orientation.

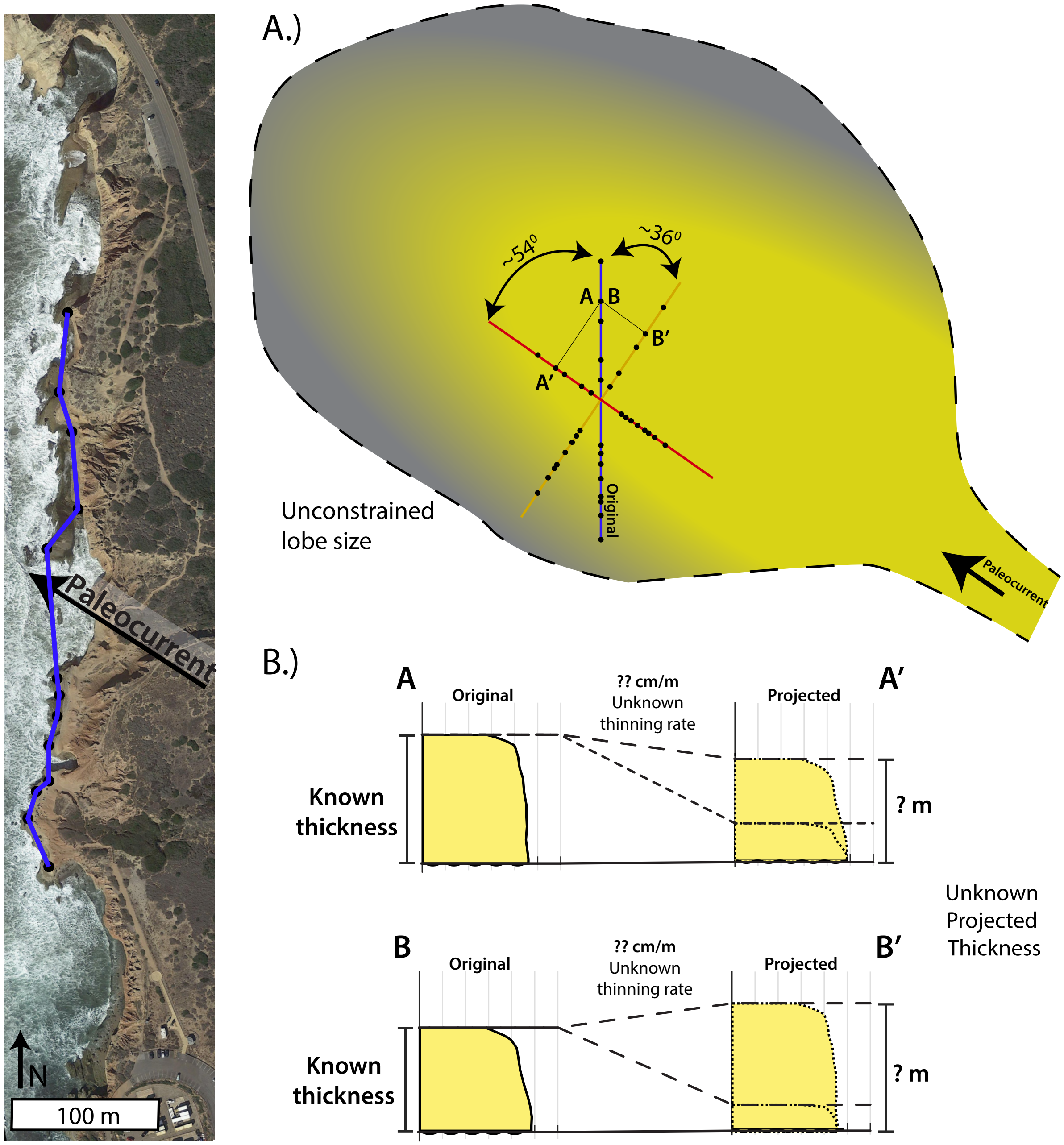

Figure 16: The error with projecting the correlation panel using the paleocurrent. Unknown bed thickness changes along the projection plane.

Supplemental Material B: Point Loma Formation Lithology and Facies Descriptions

Facies from the Cabrillo National Monument section of the Point Loma Formation are described in Table 2. This area is dominated by turbidite sandstone and mudstone couplets and contains a single hybrid event bed (Table 2). Because this project was focused on event bed variability, these facies were simplified into three lithologies (sandstone, mudstone, and debrite/hybrid beds) for ease of plotting (e.g., Figure 13 & Figure 14). This portion of the Point Loma Fm. contains a high diversity and a moderate density of bioturbation, which includes Zoophycus, Omphiomorpha, Thallisinoides, Condrites, and Skolithos (Table 2). These trace fossils correspond with previous studies at the Cabrillo National Monument and are indicative of deep water systems (Kern and Warme, 1974). Possible inoceramid shells were found in Elements One and Two, near the base of the studied section (Table 2).

Name	Description	Thickness	Degree of Bioturbation	Image
Single turbidite sandstone bed (Sand)	Light brown to tan, lower fine to lower medium base, fining upward sand beds displaying classic Bouma sequence structures (massive to parallel laminated to ripple laminated) with an erosive to loaded base. Similar to Bouma Ta, Tb, Tc and Lowe S1. Distribution of structures within bed was highly variable.	3 - 30 cm	Beds contained abundant vertical and horizontal burrows that occasionally cut through the full thickness of the bed.	
Amalgamated turbidite sandstone beds (Sand)	Light brown to tan, lower fine to lower medium base, fining upward sand beds displaying classic Bouma sequence structures (massive to parallel laminated to ripple laminated) with an erosive base. Similar to Bouma Ta,Tb,Tc and Lowe S1. Distribution of structures within bed was highly variable. Flames were present ~1/3 of the thickness up from the base and very laterally continuous. No grain size variation was across flame was documented.	5 - 20 cm	Vertical and horizontal burrows commonly found towards the top of the bed.	
Hybrid-event bed (Sand and Debrite)	Light brown to dark grey, singular bed showing lateral transition between lower medium, fining upward sand bed with classic Bouma sequence to high clay matrix with folded or contorted sand laminations. Bed also contained high amounts localized mud clasts, concretions <5cm and internal erosive features. Lateral transition was abrupt, occurring over less than 5m. Turbidite portion of the bed contained large amounts of organic material within laminations.	5 - 20 cm	Bioturbation contained within the upper ~3 cm of the turbidite sands and within contorted sand and mud clasts of the debrite.	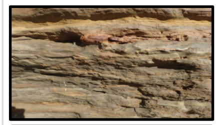 
Siltstone beds (Mud)	Grey, clay to siltstone beds that commonly showed faint wavy to parallel laminated lenses less than 5mm thick. Similar to Bouma Td, Te. Beds typically have consistent lateral thickness.	1 - 10 cm	Commonly contain small (<5mm) dark grey burrows and large (1cm) sand and mud filled burrows.	
Datum - mica rich turbidite sand with recessive clay to silt stone (Sand and Mud)	Basal light grey, parallel to ripple laminated, fine to medium sand with an erosive base. Bed thickness ranging from 1-20 cm, but is laterally continuous. Contains medium to coarse grained biotite flecks. Occasionally sheared with folded or faulted lamina. Paired with Brown to dark brown, clay to silt commonly containing sheared vertical and horizontal calcite veins. Bed thickness ranges from 5-20 cm. This recessed bed that sits directly above the mica rich bed.	6 - 40 cm	No bioturbation identified.	 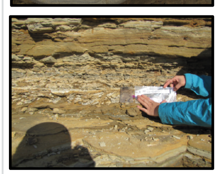

Bioturbation Images

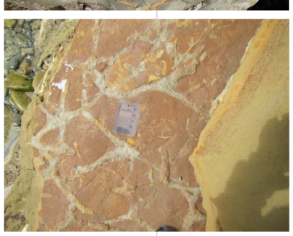

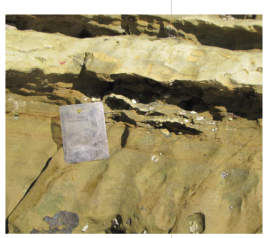

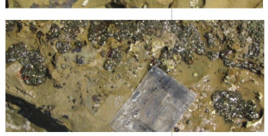

Possible Inocermid Shells

Table 2: Facies table with bioturbation images